HHS Public Access

Author manuscript

Biochim Biophys Acta Mol Cell Biol Lipids. Author manuscript; available in PMC 2020 October 01.

Published in final edited form as:

Biochim Biophys Acta Mol Cell Biol Lipids. 2019 October ; 1864(10): 1396–1411. doi:10.1016/j.bbalip.2019.05.014.

Hepatocyte peroxisome proliferator-activated receptor α regulates bile acid synthesis and transport

Cen Xie[#a,b,*], **Shogo Takahashi**[#a,c], **Chad N. Brocker**[#a], **Shijun He**[b], **Li Chen**[b,d], **Guomin Xie**[e], **Katrina Jang**[a], **Xiaoxia Gao**[a], **Kristopher W. Krausz**[a], **Aijuan Qu**[e], **Moshe Levi**[c], **Frank J. Gonzalez**[a,**]

[a]Laboratory of Metabolism, Center for Cancer Research, National Cancer Institute, National Institutes of Health, Bethesda, MD 2089, United States of America

[b]State Key Laboratory of Drug Research, Shanghai Institute of Materia Medica, Chinese Academy of Sciences, Shanghai 201203, PR China

[c]Department of Biochemistry and Molecular and Cellular Biology, Georgetown University, Washington, DC, United States of America

[d]University of Chinese Academy of Sciences, Beijing 100049, PR China

[e]Department of Physiology and Pathophysiology, School of Basic Medical Sciences, Capital Medical University, Key Laboratory of Remodeling-Related Cardiovascular Diseases, Ministry of Education, Beijing 100069, PR China

[#] These authors contributed equally to this work.

Abstract

Peroxisome proliferator-activated receptor alpha (PPARα) controls lipid homeostasis through regulation of lipid transport and catabolism. PPARα activators are clinically used for hyperlipidemia treatment. The role of PPARα in bile acid (BA) homeostasis is beginning to emerge. Herein, *Ppara*-null and hepatocyte-specific *Ppara*-null (*Ppara*$^{\Delta Hep}$) as well as the respective wild-type mice were treated with the potent PPARα agonist Wy-14,643 (Wy) and global metabolomics performed to clarify the role of hepatocyte PPARα in the regulation of BA homeostasis. Levels of all serum BAs were markedly elevated in Wy-treated wild-type mice but not in *Ppara*-null and *Ppara*$^{\Delta Hep}$ mice. Gene expression analysis showed that PPARα activation (1) down-regulated the expression of sodium-taurocholate acid transporting polypeptide and organic ion transporting polypeptide 1 and 4, responsible for the uptake of BAs into the liver; (2) decreased the expression of bile salt export pump transporting BA from hepatocytes into the bile canaliculus; (3) upregulated the expression of multidrug resistance-associated protein 3 and 4 transporting BA from hepatocytes into the portal vein. Moreover, there was a notable increase in the compositions of serum, hepatic and biliary cholic acid and taurocholic acid following Wy

[*]Correspondence to: C. Xie, State Key Laboratory of Drug Research, Shanghai Institute of Materia Medica, Chinese Academy of Sciences, Shanghai 201203, PR China. [**]Corresponding author. xiecen@simm.ac.cn (C. Xie).

Declaration of Competing Interest

The authors declare no conflict of interest.

Appendix A. Supplementary data

Supplementary data to this article can be found online at https://doi.org/10.1016/j.bbalip.2019.05.014.

treatment, which correlated with the upregulated expression of the *Cyp8b1* gene encoding sterol 12α-hydroxylase. The effects of Wy were identical between the *Ppara*$^{\Delta Hep}$ and *Ppara*-null mice. Hepatocyte PPARα controlled BA synthesis and transport not only via direct transcriptional regulation but also via crosstalk with hepatic farnesoid X receptor signaling. These findings underscore a key role for hepatocyte PPARα in the control of BA homeostasis.

Keywords

Peroxisome proliferator-activated receptor α; Wy-14; 643; Bile acid homeostasis; Farnesoid X receptor; Metabolomics

1. Introduction

Bile acids (BAs) are detergent-like molecules derived from cholesterol in the liver. The major functions of BAs include: (1) generating bile flow and inducing hepatic secretion of biliary lipids (phospholipid and cholesterol); (2) forming micelles and facilitating absorption of nutrients (lipids, cholesterol, and fat-soluble vitamins) in the gut; and (3) acting as hormones to signal through nuclear and G-protein-coupled receptors in order to regulate the bile acid enterohepatic circulation, hepatic function, gut motility, and energy metabolism [1–3]. Besides these beneficial functions, the accumulation of BAs in hepatocytes triggers cholestatic injury [4].

Hepatic BA synthesis is the predominant metabolic pathway for cholesterol catabolism in humans. BAs synthesized in the liver are designated primary BAs (cholic acid, CA, and chenodeoxycholic acid, CDCA) to distinguish them from the secondary BAs that are formed by reactions carried out by the gut microbiota [5,6]. Primary BAs are mainly synthesized via two pathways, the classic pathway and to a lesser extent the alternative pathway [7,8]. The classic (or neutral) bile acid biosynthetic pathway is initiated by the rate-limiting enzyme cholesterol 7α-hydroxylase (CYP7A1), producing most of the BA pool. Following the action of 3β-hydroxy-Δ^5-C27-steroid oxidoreductase (HSD3B7), a bile acid metabolic intermediate is further converted to CA by sterol 12α-hydroxylase (CYP8B1) and those that escape the action of CYP8B1 are transformed to CDCA by mitochondrial sterol 27-hydroxylase (CYP27A1). In this capacity, CYP8B1 controls the rate of CA synthesis and is an important determinant of the ratio of 12α-hydroxylated (12α-OH) to non-12α-OH BAs. An alternative (or acidic) pathway is initiated by CYP27A1, followed by the action of oxysterol 7α-hydroxylase (CYP7B1) to form CDCA. In rodents, another two primary BAs α- and β-muricholic acid (MCA) are generated from CDCA and ursodesoxycholic acid (UDCA) via CYP2C70-mediated 6-hydroxylation, respectively [9]. After biosynthesis, the majority of BAs are further conjugated via a two-step process involving the generation of a bile acid-CoA by bile acid-CoA synthase (BACS, SLC27A5) and then amidation with taurine (mainly in rodents) or glycine (mainly in humans) by bile acid-CoA-amino acid N-acyltransferase (BAAT) [10].

Hepatocytes take up BAs through the sinusoidal membrane which directly contacts the portal blood plasma, and excrete BAs at the canalicular membrane into bile; these are two important steps in the enterohepatic circulation of BAs [2]. Hepatocytes are polarized

epithelial cells, and thus active transport of BAs across the two membranes is required. Na^+-dependent taurocholate transporter (NTCP; SLC10A1) and organic anion transporting polypeptides (OATPs, a.k.a. SLCOs) are responsible for sinusoidal BA uptake into the hepatocytes. NTCP accounts for 80% of the total conjugated BA uptake and is regarded as the major BA uptake transporter, while OATPs mediate the uptake of the unconjugated BAs and a small fraction of conjugated BAs [11,12]. BAs are excreted into the bile canaliculi via the ATP-dependent bile salt export pump (BSEP; ABCB11). A small amount of BAs can be conjugated with sulfate or glucuronide, and then secreted primarily by multidrug resistance protein 2 (MRP2; ABCC2) [13]. The major transporters involved in hepatocyte sinusoidal bile acid efflux includes MRP3 (ABCC3), MRP4 (ABCC4), and the heteromeric organic solute transporter α-organic solute transporter β (OSTα-OSTβ; SLC51A-SLC51B) [1].

Peroxisome proliferator-activated receptor alpha (PPARα; NR1C1) is a transcription factor that responds to fatty acid metabolite agonist generated by fasting. PPARα is highly expressed in the liver, kidney, heart, skeletal muscle, and, to a lesser extent, other tissues [14–16]. Upon food deprivation or fasting, PPARα is activated and regulates lipid homeostasis through activation of genes involved in fatty acid transport and catabolism, lipoprotein metabolism, glucose homeostasis, and ketogenesis [17–19]. Moreover, during starvation, PPARα induces the expression of fibroblast growth factor (FGF) 21, which is excreted and functions as an endocrine hormone in metabolic regulation [20,21]. Fibrates have been widely used to treat hyperlipidemia for decades. They increase high-density lipoprotein levels and decreases triglyceride levels via activation of PPARα [22]. While PPARα is involved in hepatic oxidation of lipids, its role in BA synthesis and transport is much less investigated.

There is a clear relationship between hepatic PPARα and BAs, as revealed by an earlier study showing an antagonistic effect of CA and CDCA on PPARα signaling in mice [23]. Another study also showed that the natural farnesoid X receptor (FXR; NR1H4) ligand CDCA and the synthetic nonsteroidal FXR agonist GW4064 induced human *PPARA* mRNA levels in HepG2 cells [24]. Recent studies have uncovered a regulatory role for PPARα in BA homeostasis. Fibrate treatment, including bezafibrate and gemfibrozil, was found to decrease CYP7A1 expression and enzyme activity [25,26], consistent with two previous cell-based reporter assays which found that PPARα overexpression and synthetic PPARα agonist Wy-14,643 (Wy) repressed both human and rat *CYP7A1* promoter activities [27,28]. Another study revealed a contradictory result showing that both human and murine *CYP7A1* promoters were stimulated by fatty acids and Wy through PPARα [29]. *Cyp8b1* mRNA levels were induced by both 1-week Wy treatment and 24-hour fasting in the liver of wild-type mice, which is diminished in *Ppara*-null mice [30]. Expression of *Cyp27a1* was repressed by fibrate treatment in mice [31]. More recent studies revealed that activation of PPARα with clofibrate decreased expression of *Cyp7b1*, and increased expression of *Ntcp*, *Oatp4*, and *Bsep* mRNAs [32]. Although these studies provided compelling evidence demonstrating that PPARα is involved in the regulation of BA synthesis and transport, significant gaps remain in our understanding of the role of PPARα in BA homeostasis. The liver is the predominant site for BA metabolism and, to date, studies have not identified the specific regulatory mechanisms by which PPARα activation within hepatocytes influences BA homeostasis.

Therefore, the objectives of the current study are to comprehensively investigate the alterations in BA profiles in mice treated with Wy, which is a more selective and potent ligand of PPARα compared with fibrates. Mice lacking PPARα expression globally and specifically within hepatocytes were employed to clarify the effect of hepatocyte PPARα activation in BA regulation, synthesis, and transport. The physiological activation of PPARα by fasting was also evaluated.

2. Material and methods

2.1. Chemicals and reagents

Wy was purchased from Chemsyn Science Laboratories (Lenexa, KS) and mixed into a custom grain-based diet by Research Diets (New Brunswick, NJ). CA, deoxycholic acid (DCA), CDCA, taurocholic acid (TCA), taurodeoxycholic acid (TDCA), taurochenodeoxycholic acid (TCDCA), tauroursodeoxycholic acid (TUDCA), and taurohyodeoxycholic acid (THDCA) were purchased from Sigma-Aldrich (St. Louis, MO). βMCA, ω-MCA, tauro-α-muricholic acid (TαMCA), tauro-β-muricholic acid (TβMCA), and d5-TCA were obtained from Toronto Research Chemicals (North York, ON, Canada). All other reagents were of the highest grade commercially available.

2.2. Animals and treatment

Ppara wild-type ($Ppara^{+/+}$), full-body *Ppara* knockout ($Ppara^{-/-}$), *Ppara*-floxed ($Ppara^{fl/fl}$), and hepatocyte-specific *Ppara* knockout ($Ppara^{\Delta Hep}$) mice were generated and maintained as previously described [33,34]. All mice used in this study were 8- to 10-week-old males on the C57BL/6N background. Groups of $Ppara^{+/+}$ and $Ppara^{fl/fl}$ mice were included in all experiments and no detectable differences between the two control mouse strains were observed. All mice were fed ad libitum and housed in a temperature- and light-controlled vivarium in the same room and rack to avoid differences in gut microbiota. For Wy treatment, mice were allowed unrestricted access to a standard control grain diet for two weeks for acclimation, then assigned to experimental groups (6 mice per group) and placed on either a diet containing 0.1% Wy (approximately 100 mg/kg/day), or a matching grain control diet (chow) for two weeks. For the fasting study, the control group (5 mice/group) was allowed unrestricted, ad libitum access to a chow diet, while the fasting group (5 mice/group) was deprived from food, but with ad libitum access to water, for 48 h. All mouse studies were approved by the NCI Animal Care and Use Committee and performed in accordance with the Institute of Laboratory Animal Resources guidelines.

2.3. LC-MS sample preparation

BAs were extracted from mouse serum and liver tissues then analyzed by LC-MS. An aliquot of 25 μl of serum was deproteinated with 100 μl of acetonitrile containing 1 μM d5-TCA (internal standard). After centrifugation for 10 min at 15,000 ×*g*, 100 μl of the supernatant was further diluted with 100 μl of water containing 0.1% formic acid. The liver samples were homogenized with 1/10 (w/v) acetonitrile containing 1 μM d5-TCA. After centrifugation for 10 min at 15,000 ×*g*, 40 μl of supernatant was diluted with 360 μl of water containing 0.1% formic acid. A 5 μl aliquot of the supernatants was injected into an Acquity

ultra-high-performance liquid chromatography/Synapt G2Si quadrupole time-of-flight mass spectrometry system (UPLC-Q/TOF MS, Waters Corporation, Milford, MA).

2.4. BA analysis by LC-MS

BAs concentrations were measured using a Waters UPLC-Q/TOF MS system with an electrospray source. An Acquity BEH C18 column (100 × 2.1 mm internal diameter, 1.7 mm, Waters Corp.) was applied for chromatographic separation. A mixture of 0.1% formic acid in water (A) and 0.1% formic acid in acetonitrile (B) was used as the mobile phase. The gradient elution was started from 80% A for 4 min, decreased linearly to 60% A over 11 min, to 40% A over the next 5 min, to 10% A for the succeeding 1 min, and finally increased to 80% A for 4 min to re-equilibrate the column. Column temperature was maintained at 45 °C, and the flow rate was 0.4 ml/min. Mass spectrometry was carried out in the negative mode for detection of BA metabolites. A mass range of m/z 50–850 was acquired. The results were calculated according to individual standard curves established as follows: $\text{area}_{\text{analyte}}/\text{area}_{\text{internal standard}}$.

2.5. Data processing and multivariate data analysis (MDA)

Progenesis QI software (Waters Corp., Milford, MA) was used to deconvolute the chromatographic and mass spectrometric data. A multivariate data matrix containing information on sample identity, ion identity (Rt and m/z), and ion abundance was generated through centroiding, deisotoping, filtering, peak recognition, and integration. The data matrix was further analyzed using SIMCA version 14.1 software (Umetrics, Kinnelon, NJ). Principle component analysis (PCA) was used to examine the separation between groups. Orthogonal projections to latent structures discriminant analysis (OPLS-DA) was used to analyze data and identify the major latent variables in the data matrix. Potential metabolites were identified by analyzing the ions contributing to the separation of sample groups in the loading scatter plots.

2.6. Calculations of primary, secondary, 6-hydroxylated (6-OH) and 12α-OH BA concentrations

Concentrations of various BA groups including primary, secondary, 6-OH, and 12α-OH were determined by calculating the sum concentrations of the group members. The primary BAs included CA, CDCA, βMCA, TCA, TCDCA, TαMCA, and TβMCA. The secondary BAs included DCA, ωMCA, TDCA, TUDCA, and THDCA. The 6-OH BAs included βMCA, ωMCA, TαMCA, and TβMCA. The 12α-OH BAs included CA, DCA, TCA, and TDCA.

2.7. Gene expression analysis

Messenger RNA levels were measured by quantitative real-time PCR analysis using frozen liver samples processed in TRIzol reagent (Thermo-Fisher, Waltham, MA) with a Percellys bead homogenizer (Bertin, Rockville, MD) using 1 mm zirconia/silica beads. Total RNA was quantified by use of a NanoDrop spectrophotometer (NanoDrop Products, Wilmington, DE), and 2 μg of RNA reverse transcribed with cDNA Synthesis Super Mix (BioTool, Houston, TX). cDNA was quantified using SYBR Green qPCR Master Mix (BioTool,

Houston, TX) and an Applied Biosystems QuantStudio 7 Flex Real-time PCR System (Thermo-Fisher, Waltham, MA). Values are expressed as fold change over control, calculated using the 2Δ*Ct* method and normalized to *β-actin* (*Actb*) mRNA. Real-time PCR primer sequences are shown in Supplementary Table 1.

2.8. RNA sequencing (RNA-seq) analysis

Ppara$^{+/+}$ and *Ppara*$^{-/-}$ mice were placed on either control diet or matching diet containing 0.1% Wy for 48 h. Mice were killed, and livers removed for sample preparation. Thirty mg fresh liver was placed in RNAlater (Thermo-Fisher, Waltham, MA), incubated at 4 °C overnight, then stored at −80 °C. Total RNA was extracted and purified using a Qiagen RNeasy Plus kit (Qiagen, Germantown, MD) following the manufacturer's protocol. Total RNA concentrations and quality were determined. For each treatment group, total RNA from 9 to 12 mice was collected, purified, then pooled into 3 samples. Pooled total RNA samples were sent to the NCI CCR Sequencing Facility (Frederick, MD) for library preparation using TruSeq Stranded mRNA kits (Illumina, San Diego, CA) and sequencing on an Illumina HiSeq 3000 Sequencer to a depth of 50–60 million total reads per sample. Read alignment and differential gene expression analysis was performed with Qiagen CLC Genomics Workbench software.

2.9. Luciferase reporter assays

The PPAR response element (PPRE)-luciferase (PPRE-luc) construct was described previously [35]. Grace L. Guo supplied the FXR luciferase reporter construct (SHP-luc) which contains an FXR binding site from the *Nr0b2* (*Shp*) gene promoter. PPRE-luc or SHP-luc firefly luciferase reporter constructs and the phRL-TK Renilla luciferase control vector were co-transfected into AML12 hepatocytes using Lipofectamine 3000 transfection reagent (Life Technologies). Empty reporter (pGL4.10) was used as a negative control. In addition, cells were transfected with expression vectors for both mouse PPARA (pSG5-mPPARA) and FXR (pSG5-mFXR) with or without mouse RXRα (pSG5-mRXR). After transfection, cells were treated with either DMSO and/or CDCA (100 μM) and/or Wy (50 μM) for 36 h. Luciferase assays were performed using the Promega Dual-Luciferase assay kit (Madison, WI) and analyzed using a Veritas microplate luminometer (Turner Biosystems, Sunnyvale, CA).

2.10. Preparation and treatment of mouse primary hepatocytes

Mouse primary hepatocytes were isolated as described previously [9,36,37]. Hepatocytes were seeded in collagen-coated 12-well plates (Becton, Dickinson and Company, Franklin Lakes, NJ) at a density of 4×10^5 cells/well and cultured in William's E medium (Thermo Fisher Scientific) with 10% fetal bovine serum and antibiotics (100 U/ml penicillin and 100 μg/ml streptomycin, Gemini Bio Products, West Sacramento, CA). Sixteen hours after seeding, the cells were treated with medium containing 100 μM CDCA, 100 μM Wy, CDCA/Wy (each 100 μM) or dimethyl sulfoxide (DMSO) as a vehicle, respectively. For RXRα inhibition using HX531, the cells were treated with 1 μM HX531 (Tocris Bioscience, Bristol, UK) 4 h after seeding. Twelve hours after HX531 treatment, the cells were treated with medium containing 100 μM CDCA, 100 μM Wy, CDCA/Wy (each 100 μM) or dimethyl sulfoxide (DMSO) with or without 1 μM HX531, respectively. Three days after

treating the cells with the compounds, they were harvested and subjected to measurement mRNA levels.

2.11. Western blot analysis

Approximately 50 mg of mouse liver was homogenized in ice-cold buffer (0.1 M Tris-HCl, 0.1 M KCl, 1 mM EDTA, pH 7.4). The homogenates were centrifuged at 9000 *g* for 15 min at 4 °C to obtain S9 fraction. The protein concentrations of S9 fraction were measured with the Pierce BCA Protein Assay Kit (Thermo Fisher Scientific, Waltham, MA). The S9 fraction (10 μg of protein) were subjected to 4%–15% Criterion TGX Precast Midi Protein Gel (Bio-Rad, Hercules, CA) and transferred to Trans-Blot Turbo Midi polyvinylidene fluoride (Bio-Rad) using the Trans-Blot Turbo Transfer System (Bio-Rad). The membranes were blocked with 5% bovine serum albumin for 1 h and incubated overnight with primary antibodies against CYP8B1 (ab191910, 1:1000 dilution; Cambridge, United Kingdom), CYP7A1 (MABD42, 1:1000 dilution; Millipore Sigma, Burlington, MA) and the ACTB band obtained by reprobing the membranes with antibody against β-actin (#8457, 1:2000 dilution; Cell Signaling Technology, Danvers, MA), used as a loading control. Each band intensity was quantified using Bio-Rad Image Lab software, normalized by β-actin, and expressed as a fold change relative to chow-fed *Ppara*$^{fl/fl}$ mice.

2.12. Statistical analysis

Experimental values are presented as mean ± SEM. Statistical analysis was performed using Prism version 7.0 (GraphPad Software, San Diego, CA). One-way ANOVA followed by Tukey's *post-hoc* correction was applied for multi-group comparisons. *P*-values of < 0.05 were considered significant.

3. Results

3.1. Metabolomics analysis of serum from chow- and Wy-treated mice

To investigate the impact of PPARα activation on BA metabolism, untargeted metabolomics was carried out on serum from *Ppara*$^{+/+}$ and *Ppara*$^{-/-}$ mice and *Ppara*$^{fl/fl}$ and *Ppara*$^{\Delta Hep}$ mice fed a chow or matching diet containing 0.1% Wy for two weeks. Clear separation was found in the PCA plots between the chow and Wy-treated *Ppara*$^{+/+}$ mice (Fig. 1A), as well as the chow and Wy-treated *Ppara*$^{fl/fl}$ mice (Fig. 1B). Separation was also observed between the Wy-fed *Ppara*$^{+/+}$ and *Ppara*$^{-/-}$ mice (Fig. 1A), and the Wy-fed *Ppara*$^{fl/fl}$ and *Ppara*$^{\Delta Hep}$ mice (Fig. 1B). PCA analysis did not reveal major differences in the gross serum metabolite profiles of *Ppara*-null mice or *Ppara*$^{\Delta Hep}$ mice either with or without Wy treatment (Fig. 1A,B). These data indicate that BA metabolism is driven by both *Ppara* genotypes (compare *Ppara*$^{+/+}$ and *Ppara*$^{-/-}$ mice; *Ppara*$^{fl/fl}$ and *Ppara*$^{\Delta Hep}$ mice) and PPARα agonist treatment of wild-type (*Ppara*$^{+/+}$ and *Ppara*$^{fl/fl}$) mice. The agonist-derived differences are hepatocyte PPARα-dependent. Major ions driving PCA separation of chow and Wy-treated *Ppara*$^{+/+}$ mice, and the chow and Wy-treated *Ppara*$^{fl/fl}$ mice were identified based on associated loading scatter plots for *Ppara*$^{+/+}$ vs. *Ppara*$^{-/-}$ (Fig. 1C) and *Ppara*$^{fl/fl}$ vs. *Ppara*$^{\Delta Hep}$ (Fig. 1D), designated as M1 to M9. Based on the metabolomics database (https://metlin.scripps.edu), these ions were assumed to be bile acids, which were further confirmed by comparisons with authentic standards. Detailed information on these metabolites is

shown in Table 1. Taken together, PPARα activation by agonist treatment disrupted BA homeostasis, and hepatocyte PPARα plays an essential role in the regulation of bile acid homeostasis.

3.2. Effects of PPARα activation on BA concentrations and composition in mouse serum

PCA separation of groups was primarily associated with changes in BA metabolites (Table 1). Most BAs were increased in *Ppara*$^{fl/fl}$ mouse serum by Wy treatment, while no significant changes were noted in Wy-treated *Ppara*$^{\Delta Hep}$ mice (Fig. 2A). The hydrophobicity index, which reflects the hydrophilic-hydrophobic balance of total BAs and determines the rate of lipid recruitment from the liver [38], was lower in livers of *Ppara*$^{fl/fl}$ mice treated with Wy, but not *Ppara*$^{\Delta Hep}$ mice (Fig. 2B). Corresponding changes, or lack thereof, were also observed in *Ppara*$^{+/+}$ and *Ppara*$^{-/-}$ mice, respectively (Fig. S1A and B). Quantitative analysis revealed a robust increase in total BAs, conjugated BAs, and unconjugated BAs in Wy-treated *Ppara*$^{fl/fl}$ (Fig. 2C, Table S2) and *Ppara*$^{+/+}$ (Fig. S1C, Table S3) mice. Primary and secondary BAs, as well as 6-OH and 12α-OH BAs were also increased in both *Ppara*$^{fl/fl}$ and *Ppara*$^{+/+}$ mice. Serum BAs in *Ppara*$^{-/-}$ and *Ppara*$^{\Delta Hep}$ mice were not affected by agonist treatment. All these data indicate that the hepatocyte PPARα activation unbiasedly elevates all BA levels in mouse serum, most likely through regulation of BA transport.

As a percentage of total, primary BAs were increased while secondary BAs derived from gut microbiota metabolism were decreased in serum of *Ppara*$^{fl/fl}$ (Fig. 2D, Table S2) and *Ppara*$^{+/+}$ (Fig. S1D, Table S3) mice treated with Wy; no changes were observed in either *Ppara*$^{-/-}$ or *Ppara*$^{\Delta Hep}$ treatment groups. The relative proportion of each BA in the serum is shown in Fig. 2E–H and Fig. S1E–H. DCA plus TDCA were the most abundant BAs in serum of chow-fed *Ppara*$^{fl/fl}$ and *Ppara*$^{+/+}$ mice (Fig. 2E and S1E). PPARα activation by Wy treatment resulted in TCA plus CA becoming the most abundant BAs in serum (from 15.4% to 50.3% in *Ppara*$^{fl/fl}$ mice and 15.2% to 60.4% in *Ppara*$^{+/+}$ mice), whereas PPARα activation decreased DCA plus TDCA from 61.1% to 34.9% in *Ppara*$^{fl/fl}$ mice and 68.8% to 23.8% in *Ppara*$^{+/+}$ mice (Fig. 2E,F and S1E,F). However, no significant differences were noted in *Ppara*$^{-/-}$ and *Ppara*$^{\Delta Hep}$ mice by Wy treatment (Fig. 2G,H and S1G,H). These results suggest that the gut microbiota is affected in Wy-treated *Ppara*$^{+/+}$ and *Ppara*$^{fl/fl}$ mice, since DCA is produced from CA by bacterial dihydroxylation. Moreover, it appears hepatic PPARα is specifically responsible for this response as DCA does not decrease in Wy-treated *Ppara*$^{\Delta Hep}$ mice. Additionally, the concentration and relative percentage of DCA was decreased in chow-fed *Ppara*$^{-/-}$ mice compared with chow-fed *Ppara*$^{+/+}$ mice (Fig. S1A,E,G), but not in *Ppar-a*$^{\Delta Hep}$ mice (Fig. 2A,E,G), indicating that extrahepatic PPARα affected gut microbiota composition, perhaps through intestinal PPARα.

3.3. Effects of PPARα activation on BA concentrations and composition in mouse liver

Several BAs including DCA, βMCA, ωMCA, TβMCA, and THDCA were preferentially increased in livers of *Ppara*$^{\Delta Hep}$ and *Ppara*$^{-/-}$ mice treated with Wy. Except for ωMCA, all increases were modest (Figs. 3A and S2A). TCA and TCDCA, on the other hand, were increased by Wy treatment in livers of *Ppara*$^{fl/fl}$ and *Ppara*$^{+/+}$ mice, but not *Ppara*$^{\Delta Hep}$ or *Ppara*$^{-/-}$ mice (Fig. 3A and S2A). Furthermore, the hydrophobicity index was increased in livers of *Ppara*$^{fl/fl}$ and *Ppara*$^{+/+}$ mice treated with Wy, but not *Ppara*$^{\Delta Hep}$ or *Ppara*$^{-/-}$ mice

(Fig. 3B and S2B). Shifts in the major classes of BA metabolites were also observed in response to PPARα activation. The levels of all BA classes were increased in livers of Wy-treated *Ppara*$^{\Delta Hep}$ and *Ppara*$^{-/-}$ mice but not in similarly treated *Ppara*$^{fl/fl}$ or *Ppara*$^{+/+}$ mice (Fig. 3C and S2C, Table S4 and S5). However, compared to *Ppara*$^{fl/fl}$ and *Ppara*$^{+/+}$ mice, Wy treatment tended to decrease the proportion of conjugated BAs and primary BAs in livers of Wy-treated *Ppara*$^{\Delta Hep}$ and *Ppara*$^{-/-}$ mice (Fig. 3D and S2D, Table S4 and S5).

Analysis of the percentages of individual BA in the BA pool clearly revealed that TCA levels were significantly increased in livers of Wy-treated *Ppara*$^{fl/fl}$ mice, while Wy had no impact on hepatic TCA levels in *Ppara*$^{\Delta Hep}$ mice (Fig. 3E-H). Similarly, hepatic TCA fractions were elevated in Wy-treated *Ppara*$^{+/+}$ mice and unchanged in *Ppara*$^{-/-}$ mouse livers (Fig. S2E–H). In addition, the chow-fed *Ppara*$^{\Delta Hep}$ and *Ppara*$^{-/-}$ mice had lower TCA percentages in livers than the corresponding chow-fed *Ppara*$^{fl/fl}$ and *Ppara*$^{+/+}$ mice (Fig. 3E,G and S2E,G). These changes led to the PPARα-dependent alterations of percentages of 12α-OH BAs (Fig. 3D and S2D, Table S4 and S5) and the ratios of 12α-OH to non-12α-OH BAs (Fig. 3I and S2I). Furthermore, the percentages of TCDCA and TUDCA were markedly increased whereas Tα + βMCA (metabolites of TCDCA and TUDCA) were decreased by Wy treatment in livers of *Ppara*$^{fl/fl}$ and *Ppara*$^{+/+}$ mice, but not *Ppara*$^{\Delta Hep}$ or *Ppara*$^{-/-}$ mice (Fig. 3E–H and Fig. S2E–H). As a result, Wy treatment significantly decreased the percentages of 6-OH BAs in livers of *Ppara*$^{fl/fl}$ and *Ppara*$^{+/+}$ mice, but the percentages were unaffected in both knockout strains (Fig. 3D and S2D, Table S4 and S5). Taken together, these results suggest that the overall effect of hepatic PPARα activation on liver BA levels was relatively small, and the synthesis of 12α-OH BAs and 6-OH BAs seems to be controlled by hepatocyte PPARα.

3.4. Effects of PPARα activation on BA concentrations and composition in mouse gallbladder

The biliary excretion of most BA species including DCA, βMCA, ωMCA, TCA, TDCA, TCDCA, TαMCA, TβMCA, TUDCA, and THDCA was markedly decreased in *Ppara*$^{fl/fl}$ mice treated with Wy, while no significant changes were noted in Wy-treated *Ppara*$^{\Delta Hep}$ mice (Fig. 4A). The hydrophobicity index was higher in bile of *Ppara*$^{fl/fl}$ mice treated with Wy, but not *Ppara*$^{\Delta Hep}$ mice (Figs. 4B). Correspondingly, the levels of all BA classes were excreted much less in Wy-treated *Ppara*$^{fl/fl}$ mice than in chow-treated mice (Figs. 4C). These results indicate that hepatocyte PPARα activation unbiasedly reduces excretion of all BA, most likely through inhibition of BA efflux transport.

Similar to the bile acid composition in serum and liver, primary BAs were increased while secondary BAs decreased in bile of *Ppara*$^{fl/fl}$ mice treated with Wy (Fig. 4D). The relative proportion of each BA in the bile is shown in Fig. 4E-H, with taurine-conjugates as the major species of BAs in bile. PPARα activation by Wy treatment resulted in the elevation of percentages of 12α-OH BAs (Fig. 4D) and the ratios of 12α-OH to non-12α-OH BAs (Fig. 4I) by significantly increasing the TCA and TDCA fractions in bile (Fig. 4E,F). PPARα activation also significantly decreased the percentages of 6-OH BAs (Fig. 4D) as the percentages of TCDCA and TUDCA were markedly increased whereas Tα + βMCA were decreased by Wy treatment in bile of *Ppara*$^{fl/fl}$ mice, but not *Ppara*$^{\Delta Hep}$ mice (Fig. 4E-H). All

of these changes were not observed in the *Ppara*$^{\Delta Hep}$ treatment group Taken together, these results also support that the synthesis of 12α-OH BAs and 6-OH BAs is controlled by hepatocyte PPARα.

3.5. Effects of PPARα activation on expression of BA synthesis and conjugation genes

CYP8B1 regulates CA formation in the classic BA synthesis pathway and plays an important role in controlling the 12α-OH/non-12α-OH BAs ratio. *Cyp8b1* mRNA was robustly induced in *Ppara*$^{+/+}$ and *Ppara*$^{fl/fl}$ mice treated with Wy; no increase in *Cyp8b1* mRNA was found in Wy-treated knockouts (Fig. 5A,B). Notably, *Cyp8b1* expression was significantly lower in chow-fed *Ppara*$^{-/-}$ and *Ppara*$^{\Delta Hep}$ mice. The expression of CYP8B1 protein further supported the induction of CYP8B1 by hepatic PPARα activation (Fig. S3). This is consistent with ChIP-seq data (GSE61817) showing a binding peak at the CYP8B1 promoter [39], suggesting a direct transcriptional activation of *Cyp8b1* by PPARα (Fig. S4A). In contrast to *Cyp8b1*, *Cyp27a1* mRNA encoding CYP27A1 which is the rate-limiting enzyme in an alternative BA synthetic pathway that primarily contributes to CDCA formation, was similarly decreased by treatment of *Ppara*$^{+/+}$ and *Ppara*$^{fl/fl}$ mice with Wy. *Cyp27a1* expression was also PPARα-dependent as levels were unchanged in either *Ppara*$^{-/-}$ and *Ppara*$^{\Delta Hep}$ mice (Fig. 5A,B). CYP7B1 is the other important enzyme in the alternative BA synthetic pathway. *Cyp7b1* expression was markedly decreased by Wy-treatment of wild-type mice (*Ppara*$^{+/+}$ and *Ppara*$^{fl/fl}$) mice with no decreased in this mRNA after Wy-treatment in either knockout mouse line (Fig. 5A,B). Interestingly, *Cyp7b1* expression was constitutively elevated in chow fed *Ppara*$^{-/-}$ and *Ppara*$^{\Delta Hep}$ mice. CYP2C70 is involved in the conversion of CDCA to MCA [9]. *Cyp2c70* mRNA expression was substantially decreased in both wild-type mouse lines (*Ppara*$^{+/+}$ and *Ppara*$^{fl/fl}$) treated with Wy (Fig. 5A,B). Like *Cyp27a1* and *Cyp7b1*, *Cyp2c70* mRNA suppression was hepatocyte PPARα-dependent. Lower CYP2C70 protein would provide a mechanistic explanation for the decrease TβMCA fractions after Wy treatment in *Ppara*$^{+/+}$ and *Ppara*$^{fl/fl}$ mice. *Hsd3b7* mRNA was also slightly elevated in livers of Wy-treated *Ppara*$^{+/+}$ and *Ppara*$^{fl/fl}$ mice and not in *Ppara*$^{-/-}$ or *Ppara*$^{\Delta Hep}$ mice, and *Cyp7a1* mRNA, which encodes the rate-limiting enzyme in BA synthesis, was unchanged by Wy (Fig. 5A,B). CYP7A1 protein was also unchanged by Wy treatment of *Ppara*$^{\Delta Hep}$ mice (Fig. S3).

Analysis of mRNA for other enzymes involved in the synthesis of taurine conjugates revealed that *Csad* mRNA was increased while *Taut* (a.k.a. *Slc6a6*), *Cdo* (a.k.a. *Cdo1*), *Bacs*, and *Baat* were decreased in Wy-treated *Ppara*$^{+/+}$ and *Ppara*$^{fl/fl}$ mice (Fig. 5C,D). Except for *Cdo* mRNA, which was slightly increased by Wy, *Csd*, *Taut*, *Bacs*, and *Baat* mRNAs were unchanged in Wy-treated *Ppara*$^{-/-}$ and *Ppara*$^{\Delta Hep}$ mice. Overall, these results revealed a functional role of hepatocyte PPARα in BA synthesis and conjugation.

3.6. Effects of PPARα activation on gene expression of hepatic and biliary BA transport system

For sinusoidal transporters, treatment of *Ppara*$^{+/+}$ and *Ppara*$^{fl/fl}$ mice with Wy decreased the mRNA expression of the conjugated BA uptake transporter NTCP, and the unconjugated BA transporters OATP1 and OATP4, and increased mRNAs encoding the efflux transporters MRP3 and MRP4 (Fig. 5E,F). Activation or suppression of these genes were PPARα-

dependent as expression was unchanged or showed opposite alterations in Wy-treated *Ppara*$^{-/-}$ or *Ppara*$^{\Delta Hep}$ mice. Analysis of archived PPARα ChIP-seq datasets (GSE61817) indicated a binding peak at the *Mrp4* promoter [39], suggesting direct transcriptional activation of *Mrp4* by PPARα (Fig. S4B). These data suggest that following PPARα activation by Wy, serum BA levels are increased through decreased expression of the hepatic BA uptake and increased BA transport back to circulation. Expression of the canalicular transporter BSEP contributes to BA pool size by facilitating BA transport from hepatocytes into the bile. *Bsep* mRNA was substantially decreased by Wy treatment in wild-type (*Ppara*$^{+/+}$ and *Ppara*$^{fl/fl}$) mice (Fig. 5G,H). The mRNA level of the other BA efflux transport MRP2 was slightly induced by Wy (Fig. 5G,H). *Abcg5* and *Abcg8* encode canalicular heterodimer cholesterol efflux transporters and *Mdr2* (*Abcb4*, *MDR3* in humans) encodes a canalicular phospholipid efflux transporter [40,41]. *Abcg5*, *Abcg8*, and *Mdr2* mRNAs were significantly upregulated by PPARα activation in *Ppara*$^{+/+}$ and *Ppara*$^{fl/fl}$. Levels of these canalicular transporter mRNAs were unchanged in Wy-treated knockout models indicating that these changes are either directly or indirectly dependent on PPARα (Fig. 5G,H). These data suggest that hepatocyte PPARα appears to be involved in the regulation of BA transport.

3.7. Effects of PPARα activation on gene expression of BA homeostasis regulation

Changes in levels of BA metabolites may affect signaling from other receptors that are modulated by BAs either directly or indirectly. FXR is directly activated by BAs and primarily regulates BA transport and synthesis through a complex network of transcriptional cascades that mediate enterohepatic circulation [42]. BAs also indirectly regulate liver receptor homologue 1 (LRH1; NR5A2) and hepatocyte nuclear factor 4α (HNF4α; NR2A1), which are positive regulators of BA synthesis [43,44]. Along with the activation of hepatic PPARα signaling by Wy (Fig. 6A), hepatic *Fxr* mRNA was not altered in *Ppara*$^{fl/fl}$ treated with Wy, while the FXR target gene small heterodimer partner (*Shp*) mRNA was markedly decreased indicating FXR signaling may be attenuated (Fig. 6B). Moreover, *Lrh1* and *Hnf4a* mRNAs were also decreased in *Ppara*$^{fl/fl}$ mice treated with Wy (Fig. 6B). These changes are not observed in Wy-treated *Ppara*$^{\Delta Hep}$ mice. These findings implied that PPARα regulates BA synthesis and transport at least partially through affecting liver FXR signaling. Wy also activated intestinal PPARα as revealed by a significantly induction in the PPARα target gene mRNAs *Acot1* and *Cyp4a10* (Fig. 6C) while intestinal FXR signaling was suppressed as reflected by decreased *Fgf15* mRNA, an FXR target gene, in both *Ppara*$^{fl/fl}$ and *Ppara*$^{\Delta Hep}$ mice (Fig. 6D). Meanwhile, Wy treatment inhibited intestinal BA absorption by downregulation of *Asbt* and *Ibabp* mRNAs in both *Ppara*$^{fl/fl}$ and *Ppara*$^{\Delta Hep}$ mice (Fig. 6D). These data suggested that inhibition of intestinal FXR by Wy treatment is not mediated by hepatic PPARα and that the intestinal FXR-FGF15 axis is not required for hepatic PPARα-controlled BA metabolism.

Since the proportion of hepatic BAs with FXR agonistic potency (CA, TCA, and TCDCA) were significantly elevated and those with FXR antagonistic potency (TαMCA, TβMCA) were decreased in Wy-treated mice, the BA pool would be expected to activate hepatic FXR signaling. However, the current data showed that hepatic PPARα activation repressed the FXR-SHP pathway. To explore how PPARα modulates FXR signaling, primary hepatocytes

were isolated from wild-type, *Ppara*$^{-/-}$, and *Fxr*$^{-/-}$ mice and treated with CDCA, Wy, or the combination of CDCA and Wy. CDCA suppressed Wy-induced PPARα activation as illustrated by the mRNA levels of two PPARα target genes *Acox1* and *Cyp4a10* (Fig. S5A–C), while Wy suppressed CDCA-induced FXR activation revealed by the mRNA levels of two FXR target genes *Shp* and *Bsep* (Fig. S5D–F). These effects were abrogated in either *Ppara*$^{-/-}$ or *Fxr*$^{-/-}$ mice. To understand the mechanism for the interplay between PPARα and FXR, cell-based luciferase reporter assays were carried out. PPRE-luc or SHP-luc firefly luciferase reporter constructs were transiently co-transfected into AML12 hepatocytes with empty vector or both FXR and PPARα expression vectors with or without a retinoid X receptor α (RXRα; NR2B1) expression vector. In the PPARα reporter assay system, PPARα activation by Wy dramatically increased luciferase activity of the PPRE-luc reporter, whereas FXR agonist CDCA co-treatment significantly suppressed Wy-activated PPARα transcriptional activity (Fig. 6E). Similarly, luciferase activity of the SHP-luc reporter was notably induced by CDCA treatment but attenuated by adding Wy into the FXR reporter assay system (Fig. 6F). Interestingly, expressing a surplus of RXRα negated the decrease in luciferase activities in both systems indicating that the pool of unbound RXRα is limiting (Fig. 6E and F). To further clarify the role of RXRα competition in PPARα and FXR crosstalk, RXRα inhibitor HX531 was used to deplete the RXRα pool in primary hepatocytes. HX531 treatment decreased the CDCA-induced *Shp* mRNA levels in both wild type and *Ppara*$^{-/-}$ primary hepatocytes, and abolished the suppressive effects of Wy (Fig. S5G and H). These results suggest a crosstalk between PPARα and FXR, potentially through RXRα competition.

3.8. RNA-seq analysis of livers from short-term Wy-treated mice

To exclude the unexpected secondary regulatory effects following long-term Wy feeding on PPARα activation and figure out the exact role of PPARα activation on BA homeostasis, RNA-seq analysis was performed on the livers from 48-hour Wy-treated mice. Expression of *Shp*, *Cyp27a1*, *Cyp7b1*, *Cyp2c70*, *Taut*, *Cdo*, *Bacs*, *Baat*, *Ntcp*, *Oatp1*, *Oatp4*, *Ostb*, and *Bsep* mRNAs were downregulated, while the expression of *Cyp8b1*, *Csad*, *Mrp3*, *Mrp4* and *Mdr2* mRNAs were upregulated by Wy treatment (Fig. S6). These alterations were ablated in *Ppara*$^{-/-}$ mice, except for *Mrp4* mRNA which exhibited an attenuated response. *Mrp4* mRNA was only induced 1.8-fold in Wy-treated knockout mice when compared to 4.2-fold in Wy-treated wild-type mice. These results implied an early occurrence of crosstalk between PPARα and FXR resulting in a rapid regulation of bile acid synthesis and transport.

3.9. Effects of physiological PPARα activation by fasting on BA concentrations and composition

To further elucidate the role of PPARα activation in BA metabolism, the mice were fasted for 48 h to physiological activate PPARα. Compared to Wy treatment, fasting had similar effects on serum and liver BA profiles in *Ppara*$^{fl/fl}$ mice resulting in increased individual, total, and other classes of BAs in serum, lowered hydrophobicity index, and increased percentages of TCA plus CA and the ratios of 12α-OH to non-12α-OH BAs (Fig. 7 and Fig. 8). However, compared to the fasted-*Ppara*$^{fl/fl}$ mice, hepatic PPARα disruption further increased serum BA levels by 2-fold, but did not affect serum BA composition (Fig. 7). Contrasting the increase of hepatic BAs in Wy-treated *Ppara*$^{\Delta Hep}$ mice, there was no

difference between fed and fasted *Ppara*$^{\Delta Hep}$ mice (Fig. 8A,C). Gene expression analysis showed that fasting inhibited FXR signaling and altered multiple genes involved in BA metabolism and transport, as did Wy treatment (Fig. S7). However, fasting further induced *Mrp3* and *Mrp4* mRNA levels leading to the accumulation of BAs in the serum of *Ppara*$^{\Delta Hep}$ mice. These data indicate that physiological activation of hepatic PPARα by fasting has similar effects on BA synthesis and transport as pharmacological activation of PPARα by Wy. However, fasting also has other effects that need to be further explored.

4. Discussion

The liver plays a central role in maintaining BA homeostasis. It was shown that PPARα activators, such as Wy and fibrates disrupt BA homeostasis in mice [31,32,45,46]. However, these studies cannot distinguish the direct regulatory effects from hepatic PPARα and the indirect effects from PPARα expressed in extrahepatic tissues. Therefore, it is important to investigate the impact of hepatocyte-specific PPARα deletion on BA profiles in vivo. Herein, Wy treatment remarkably elevated the levels of all the BAs in serum as well as increased ratios of the CA-derived 12α-OH/CDCA-derived non-12α-OH BAs via the regulation of many genes involved in BA metabolism and transport. The alterations in BA homeostasis observed in wild-type mice were almost ablated in both full body knockout and hepatocyte-specific knockout mice (Fig. 9). This is the first report showing that PPARα expression and activation specifically within hepatocytes plays an important role in the regulation of BA synthesis and transport.

The current study revealed that PPARα activation has a profound impact on BA homeostasis and caused a pronounced increase in circulating BA levels, since Wy treatment resulted in a 12.4-fold and 16.8-fold increase in total BAs in *Ppara*$^{fl/fl}$ and *Ppara*$^{+/+}$ mice, respectively. CYP7A1 is the first and key enzyme in bile acid synthesis, determining the size of BA pool in vivo [1]. To date, conflicting results were reported on the effects of PPARα agonists on the expression and activity of CYP7A1 [25–29]. In the current study, the levels of *Cyp7a1* mRNA were unchanged in all treatment groups. Moreover, the total BAs in the livers of *Ppara*$^{fl/fl}$ and *Ppara*$^{+/+}$ mice remained unchanged in response to Wy treatment. These observations suggest that the regulatory function of PPARα has more impact on the serum BA pool than the liver, most likely due to the regulation of BA transport. Indeed, PPARα activation by Wy increases circulating BA levels by decreasing expression of the mRNAs encoding the sinusoidal uptake transporters NTCP and OATPs, while at the same time, increasing expression of the mRNAs encoding the efflux transporters MRP3 and MRP4. Meanwhile, PPARα activation also down-regulates expression of the major canalicular efflux transporter BSEP, maintaining hepatic BA levels at normal levels. These changes were blocked in Wy-treated *Ppara*$^{-/-}$ or *Ppara*$^{\Delta Hep}$ mice. Several studies have implicated that PPARα may be involved in the regulation of BA transport in the liver. Two weeks' ciprofibrate feeding was shown to significantly decrease hepatic NTCP, OATP1, BSEP expression in mice with reduced biliary BA concentrations [47]. Another study also demonstrated a PPARα-dependent down-regulation of OATPs and NTCP by perfluorinated fatty acids [48]. On the contrary, a recent study revealed that short-term (4 days) clofibrate treatment increased the mRNA expression of *Ntcp*, *Oatp4*, and *Bsep* in mice [32]. To explain these contradicting observations, the BA transport-related genes were screened in the RNA-

seq dataset of the livers from 48-hour Wy-treated mice in the present study to exclude the potential prolonged effects induced by Wy treatment. Consistent with the present long-term treatment results, short-term Wy feeding also decreased the expression of *Ntcp*, *Oatp1*, *Oatp4*, and *Bsep* mRNAs, while increasing the expression of *Mrp3* and *Mrp4* mRNAs. This discrepancy may be explained by clofibrate activating PPARα in muscle, liver, and other tissues, whereas Wy is a more potent and selective ligand for PPARα compared with fibrates which primarily activate hepatic PPARα [49,50]. Furthermore, upregulation of the sinusoidal export pumps MRP3 and MRP4 presumably functions as an adaptive compensatory mechanism to reduce the damaging cellular effects of cholestasis. *Mrp4*-null mice displayed more severe liver injury after bile duct ligation, along with significant reductions in serum BA levels [51]. PPARα could directly activate *Mrp4* transcription because a binding peak was noted in the archived PPARα ChIP-seq datasets (GSE61817). These findings have led to the idea that pharmacological upregulation of MRP3 and MRP4 might be of therapeutic benefit.

Elevated BA content revealed a significant shift in relative concentrations towards TCA and CA in both serum and liver. The ratio of 12α-OH/non-12α-OH BA metabolites within the total BA pool also increased in response to PPARα activation. The present data indicates that upregulation of CYP8B1 in the classic pathway for CA formation and downregulation of CYP27A1 and CYP7B1 in the alternative pathway for CDCA formation may be responsible for this alteration. Regulation of CYP8B1 was PPARα-dependent as expression in *Ppara* knockout mouse lines was unchanged. Analysis of the ChIP-seq dataset identified a strong binding site within the *Cyp8b1* promoter region suggesting that this gene is directly regulated by PPARα. This was supported by an early study where a functional PPRE was identified in the rat *CYP8B1* promoter region in HepG2 cells [30]. It was also reported that bezafibrate treatment can increase CA to CDCA ratios in gallstone patients, which further supports that regulation of CYP8B1 by PPARα may likely be conserved in humans [25]. In line with the current observations, fibrate treatment reduced *Cyp27a1* and *Cyp7b1* mRNA expression in the liver, which were completely abolished in *Ppara*-null mice [31,32]. Furthermore, PPARα activation decreases rodent-specific BA Tα + βMCA levels and increases TCDCA levels by suppressing expression of *Cyp2c70*. The mechanism by which *Cyp2c70* mRNA is decreased by PPARα activation remains to be elucidated.

Changes in relative local concentrations of endogenous BA agonists and antagonists in hepatocytes may affect the activity of FXR, which is tightly linked to BA metabolism and transport [3]. In the current study, the relative levels of FXR agonist pool (CA, TCA, and TCDCA) were increased while the FXR antagonist pool (TαMCA and TβMCA) were decreased in livers from Wy-treated wild-type mice, indicating the possibility of BA-activated FXR signaling by PPARα activation. Nonetheless, PPARα activation by Wy is coincident with inhibition of FXR signaling as revealed by a decrease in the FXR target gene *Shp*. This can be explained by the crosstalk between PPARα and FXR through RXRα competition which was further confirmed by using cell-based luciferase reporter assays and RXRα inhibition studies. Wy treatment strongly activates PPARα dramatically reducing unbound RXRα pools within hepatocytes. The depletion of RXRα by Wy occurs as early as 48 h after treatment as the expression of *Shp* was reduced in 48-h Wy-treated mice. By outcompeting FXR for RXR, PPARα activation indirectly suppresses FXR signaling,

whereas PPARα disruption would not markedly alter RXRα levels in hepatocytes and thus FXR was not notably activated in *Ppara* knockouts. *Ntcp*, *Oatp1*, *Oatp4*, and *Bsep* are known target genes of FXR [42]. Therefore, FXR inhibition by PPARα activation is likely responsible for the observed down-regulated of these transporters.

Two mechanisms have been proposed for FXR feedback inhibition of CYP7A1, CYP8B1, and bile acid synthesis. In the liver, binding of BAs to FXR-RXRα heterodimer results in transcription of SHP, a transcriptional co-repressor, which inhibits *CYP7A1* and *CYP8B1* gene expression by preventing the LRH1- and/or HNF4α-mediated induction of these genes [43,52]. In addition to the local effect in the liver, FXR in the distal ileum is also activated by BAs and then induces FGF15, which circulates to the liver and binds to FGF receptor 4/β-Klotho heterodimer, thereby inhibiting *CYP7A1* and *CYP8B1* gene transcription via JNK and ERK signaling cascade [53]. In the current study, suppression of the FXR-SHP pathway would be expected to cause upregulation of both *Cyp7a1* and *Cyp8b1*. However, the mRNA levels of *Lrh1* and *Hnf4a* were reduced by Wy, independent of the action of the co-repressor SHP. As a result, *Cyp7a1* gene expression was not affected by either PPARα activation or disruption. This is consistent with a previous finding that 1-week Wy feeding did not alter *Cyp7a1* mRNA [31]. Furthermore, Wy treatment was found to downregulate *Fgf15* expression via intestinal PPARα-FXR competition. Thus, neither hepatic nor intestinal FXR signaling was involved in the regulation of CYP7A1 after Wy treatment. However, in addition to the direct transcriptional control by PPARα, it seems that the hepatic FXR/SHP pathway and intestine-derived FGF15 are also responsible for the induction of CYP8B1 by PPARα activation. Recent studies reported that induction of CYP8B1 and increased 12-OH BAs are linked to NAFLD and insulin resistance [54–56], implying that hepatic PPARα activation may have a negative effect on lipogenesis and glucose metabolism.

In addition to pharmacological PPARα activation by Wy, physiological activation of PPARα by fasting also has similar effects on BA metabolism and transport. However, there was still some hepatic PPARα-independent effects because the BA balance was still disrupted in the $Ppara^{\Delta Hep}$ mice. Besides hepatic PPARα, extrahepatic PPARα and other nutrient-sensing nuclear receptors like PXR, LXR and FXR also control the response to fasting [57].

It is known that the hydrophilic-hydrophobic balance of secreted BAs in the BA pool may have a close relationship to cholesterol and lipid absorption efficiency. Hydrophobic BAs have a high capability for solubilizing fats and lipids while the hydrophilic BAs preclude efficient sterol solubilization [58]. PPARα activation by Wy was shown to increase the hydrophobicity index of BA pool implying a potentially decreased lipid and cholesterol absorption. Moreover, the canalicular cholesterol transporters (ABCG5 and ABCG8) and phospholipid efflux transporter MDR2 were also induced by PPARα activation. These observations suggest that the lipid- and cholesterol-lowering effects of PPARα agonists might be partially mediated though PPARα-BA axis via decreased absorption in the intestine.

The effects of Wy on BA homeostasis were completely negated in hepatocyte-specific *Ppara* knockout mice and corresponded to data from full-body knockout mice. This strongly indicates that PPARα activation within hepatocytes contributes to maintaining BA

homeostasis. The current data also suggests that crosstalk with FXR may further lead to alterations in BA metabolites. Here, an important role of PPARα was uncovered in the regulation of genes encoding proteins responsible for bile acid synthesis and transport in humans, including CYP8B1, NTCP, BSEP, MRP3 and MRP4. Expression of many of these genes is altered in cholestatic liver diseases. Accumulating data demonstrated that PPARα activation by fibrates has beneficial effects on cholestatic diseases in humans and experimental animal models. Bezafibrate improved cholestasis-related marker serum alkaline phosphatase in patients with hyperlipidemia [59]. Fenofibrate is increasingly used to treat patients with chronic cholestatic liver diseases who are refractory to UDCA monotherapy [50]. Moreover, fenofibrate protected against ANIT-induced intrahepatic cholestatic liver injury [60,61]. Fenofibrate, bezafibrate, or gemfibrozil attenuated the acute cholestasis induced by ethinylestradiol plus chlorpromazine in rats [62]. Together these observations introduce the possibility that PPARα ligands could be beneficial, and considered as an alternative pharmacological target, for the treatment of various cholestatic liver disorders.

Supplementary Material

Refer to Web version on PubMed Central for supplementary material.

Acknowledgments

This study was partially supported by the National Cancer Institute Intramural Research Program NIH R01 AG049493 and NIH R01 DK116567. C.N.B. was supported in part by the Postdoctoral Research Associate Training (PRAT) program through the National Institute of General Medical Sciences, National Institutes of Health. Xiaoxia Gao was supported by a fellowship from Shanxi University. We thank Yuhong Luo providing mice and Linda G. Byrd for preparing the animal protocols.

Abbreviations

BA	bile acid
BAAT	bile acid-CoA:amino acid N-acyltransferase
BACS	bile acid-CoA synthetase
BSEP	bile salt export pump
CA	cholic acid
CDCA	chenodeoxychoic acid
CDO	cysteine dioxygenase
CSD	cysteinesulfinate decarboxylase
CYP	cytochrome P450
DCA	deoxycholic acid
FXR	farnesoid X receptor

HSD	hydroxysteroid dehydrogenase
HNF4α	hepatocyte nuclear receptor 4α
LRH1	liver receptor homologue 1
βMCA	β-muricholic acid
ωMCA	ω-muricholic acid
MDA	multivariate data analysis
MRP	multidrug resistant protein
NTCP	Na^+-dependent taurocholate transporter
OATP	organic anion transporting polypeptides
OPLS-DA	Orthogonal projections to latent structures discriminant analysis
OST	organic solute transporter
PCA	principal components analysis
PPARα	peroxisome proliferator-activated receptor α
Q/TOF MS	quadrupole time-of-flight mass spectrometry
RXR	retinoid X receptor
SNP	small heterodimer partner
NTCP	sodium-taurocholate acid transporting polypeptide
TAUT	taurine transporter
TαMCA	tauro-α-muricholic acid
TβMCA	tauro-β-muricholic acid
TCDCA	taurochenodeoxycholic acid
TCA	taurocholic acid
TDCA	taurodeoxycholic acid
THDCA	taurohyodeoxycholic acid
TUDCA	tauroursodeoxycholic acid
UPLC	high performance chromatography
Wy	Wy-14643

References

[1]. Dawson PA, Bile formation and the enterohepatic circulation, Physiology of the Gastrointestinal Tract, Sixth edition, Elsevier, 2018, pp. 931–956.

[2]. Li T, Chiang JY, Regulation of bile acid and cholesterol metabolism by PPARs, PPAR Res. 2009 (2009) 501739.

[3]. Chavez-Talavera O, Tailleux A, Lefebvre P, Staels B, Bile acid control of metabolism and inflammation in obesity, type 2 diabetes, dyslipidemia, and nonalcoholic fatty liver disease, Gastroenterology 152 (2017) 1679–1694 (e1673). [PubMed: 28214524]

[4]. Perez MJ, Briz O, Bile-acid-induced cell injury and protection, World J. Gastroenterol. 15 (2009) 1677–1689. [PubMed: 19360911]

[5]. Dawson PA, Karpen SJ, Intestinal transport and metabolism of bile acids, J. Lipid Res. 56 (2015) 1085–1099. [PubMed: 25210150]

[6]. Ridlon JM, Harris SC, Bhowmik S, Kang DJ, Hylemon PB, Consequences of bile salt biotransformations by intestinal bacteria, Gut Microbes 7 (2016) 22–39. [PubMed: 26939849]

[7]. Chiang JY, Bile acids: regulation of synthesis, J. Lipid Res. 50 (2009) 1955–1966. [PubMed: 19346330]

[8]. Qi Y, Jiang C, Cheng J, Krausz KW, Li T, Ferrell JM, Gonzalez FJ, Chiang JY, Bile acid signaling in lipid metabolism: metabolomic and lipidomic analysis of lipid and bile acid markers linked to anti-obesity and anti-diabetes in mice, Biochim. Biophys. Acta 1851 (2015) 19–29. [PubMed: 24796972]

[9]. Takahashi S, Fukami T, Masuo Y, Brocker CN, Xie C, Krausz KW, Wolf CR, Henderson CJ, Gonzalez FJ, Cyp2c70 is responsible for the species difference in bile acid metabolism between mice and humans, J. Lipid Res. 57 (2016) 2130–2137. [PubMed: 27638959]

[10]. Pircher PC, Kitto JL, Petrowski ML, Tangirala RK, Bischoff ED, Schulman IG, Westin SK, Farnesoid X receptor regulates bile acid-amino acid conjugation, J. Biol. Chem 278 (2003) 27703–27711. [PubMed: 12754200]

[11]. Kouzuki H, Suzuki H, Ito K, Ohashi R, Sugiyama Y, Contribution of sodium taurocholate co-transporting polypeptide to the uptake of its possible substrates into rat hepatocytes, J. Pharmacol. Exp. Ther 286 (1998) 1043–1050. [PubMed: 9694967]

[12]. van de Steeg E, Wagenaar E, van der Kruijssen CM, Burggraaff JE, de Waart DR, Elferink RP, Kenworthy KE, Schinkel AH, Organic anion transporting polypeptide 1a/1b-knockout mice provide insights into hepatic handling of bilirubin, bile acids, and drugs, J. Clin. Invest 120 (2010) 2942–2952. [PubMed: 20644253]

[13]. Lefebvre P, Cariou B, Lien F, Kuipers F, Staels B, Role of bile acids and bile acid receptors in metabolic regulation, Physiol. Rev 89 (2009) 147–191. [PubMed: 19126757]

[14]. Yang Q, Nagano T, Shah Y, Cheung C, Ito S, Gonzalez FJ, The PPARα-humanized mouse: a model to investigate species differences in liver toxicity mediated by PPARα, Toxicol. Sci 101 (2008) 132–139. [PubMed: 17690133]

[15]. Cheung C, Gonzalez FJ, Humanized mouse lines and their application for prediction of human drug metabolism and toxicological risk assessment, J. Pharmacol. Exp. Ther 327 (2008) 288–299. [PubMed: 18682571]

[16]. Brocker CN, Patel DP, Velenosi TJ, Kim D, Yan T, Yue J, Li G, Krausz KW, Gonzalez FJ, Extrahepatic PPARα modulates fatty acid oxidation and attenuates fasting-induced hepatosteatosis in mice, J. Lipid Res. 59 (2018) 2140–2152. [PubMed: 30158201]

[17]. Issemann I, Green S, Activation of a member of the steroid hormone receptor superfamily by peroxisome proliferators, Nature 347 (1990) 645–650. [PubMed: 2129546]

[18]. Aoyama T, Peters JM, Iritani N, Nakajima T, Furihata K, Hashimoto T, Gonzalez FJ, Altered constitutive expression of fatty acid-metabolizing enzymes in mice lacking the peroxisome proliferator-activated receptor α (PPARα), J. Biol. Chem 273 (1998) 5678–5684. [PubMed: 9488698]

[19]. Pyper SR, Viswakarma N, Yu S, Reddy JK, PPARα: energy combustion, hypolipidemia, inflammation and cancer, Nucl. Recept. Signal 8 (2010) e002.

[20]. Badman MK, Pissios P, Kennedy AR, Koukos G, Flier JS, Maratos-Flier E, Hepatic fibroblast growth factor 21 is regulated by PPARα and is a key mediator of hepatic lipid metabolism in ketotic states, Cell Metab. 5 (2007) 426–437. [PubMed: 17550778]

[21]. Inagaki T, Dutchak P, Zhao G, Ding X, Gautron L, Parameswara V, Li Y, Goetz R, Mohammadi M, Esser V, Elmquist JK, Gerard RD, Burgess SC, Hammer RE, Mangelsdorf DJ, Kliewer SA, Endocrine regulation of the fasting response by PPARα-mediated induction of fibroblast growth factor 21, Cell Metab. 5 (2007) 415–425. [PubMed: 17550777]

[22]. Fruchart JC, Duriez P, Mode of action of fibrates in the regulation of triglyceride and HDL-cholesterol metabolism, Drugs Today (Barc) 42 (2006) 39–64. [PubMed: 16511610]

[23]. Sinal CJ, Yoon M, Gonzalez FJ, Antagonism of the actions of peroxisome proliferator-activated receptor-α by bile acids, J. Biol. Chem 276 (2001) 47154–47162. [PubMed: 11606578]

[24]. Pineda Torra I, Claudel T, Duval C, Kosykh V, Fruchart JC, Staels B, Bile acids induce the expression of the human peroxisome proliferator-activated receptor α gene via activation of the farnesoid X receptor, Mol. Endocrinol 17 (2003) 259–272. [PubMed: 12554753]

[25]. Stahlberg D, Reihner E, Rudling M, Berglund L, Einarsson K, Angelin B, Influence of bezafibrate on hepatic cholesterol metabolism in gallstone patients: reduced activity of cholesterol 7α-hydroxylase, Hepatology 21 (1995) 1025–1030. [PubMed: 7705775]

[26]. Bertolotti M, Concari M, Loria P, Abate N, Pinetti A, Guicciardi ME, Carulli N, Effects of different phenotypes of hyperlipoproteinemia and of treatment with fibric acid derivatives on the rates of cholesterol 7α-hydroxylation in humans, Arterioscler. Thromb. Vasc. Biol 15 (1995) 1064–1069. [PubMed: 7627697]

[27]. Marrapodi M, Chiang JY, Peroxisome proliferator-activated receptor α (PPARα) and agonist inhibit cholesterol 7α-hydroxylase gene (CYP7A1) transcription, J. Lipid Res 41 (2000) 514–520. [PubMed: 10744771]

[28]. Patel DD, Knight BL, Soutar AK, Gibbons GF, Wade DP, The effect of peroxisome-proliferator-activated receptor-α on the activity of the cholesterol 7α-hydroxylase gene, Biochem. J 351 (Pt 3) (2000) 747–753. [PubMed: 11042130]

[29]. Cheema SK, Agellon LB, The murine and human cholesterol 7α-hydroxylase gene promoters are differentially responsive to regulation by fatty acids mediated via peroxisome proliferator-activated receptor α, J. Biol. Chem 275 (2000) 12530–12536. [PubMed: 10777541]

[30]. Hunt MC, Yang YZ, Eggertsen G, Carneheim CM, Gafvels M, Einarsson C, Alexson SE, The peroxisome proliferator-activated receptor alpha (PPARα) regulates bile acid biosynthesis, J. Biol. Chem 275 (2000) 28947–28953. [PubMed: 10867000]

[31]. Post SM, Duez H, Gervois PP, Staels B, Kuipers F, Princen HM, Fibrates suppress bile acid synthesis via peroxisome proliferator-activated receptor-α-mediated downregulation of cholesterol 7α-hydroxylase and sterol 27-hydroxylase expression, Arterioscler. Thromb. Vasc. Biol 21 (2001) 1840–1845. [PubMed: 11701475]

[32]. Zhang Y, Lickteig AJ, Csanaky IL, Klaassen CD, Editor's highlight: Clofibrate decreases bile acids in livers of male mice by increasing biliary bile acid excretion in a PPARα-dependent manner, Toxicol. Sci 160 (2017) 351–360. [PubMed: 28973556]

[33]. Lee SS, Pineau T, Drago J, Lee EJ, Owens JW, Kroetz DL, Fernandez-Salguero PM, Westphal H, Gonzalez FJ, Targeted disruption of the α isoform of the peroxisome proliferator-activated receptor gene in mice results in abolishment of the pleiotropic effects of peroxisome proliferators, Mol. Cell. Biol 15 (1995) 3012–3022. [PubMed: 7539101]

[34]. Brocker CN, Yue J, Kim D, Qu A, Bonzo JA, Gonzalez FJ, Hepatocyte-specific PPARA expression exclusively promotes agonist-induced cell proliferation without influence from nonparenchymal cells, Am. J. Physiol. Gastrointest. Liver Physiol 312 (2017) G283–g299.

[35]. Kim JB, Wright HM, Wright M, Spiegelman BM, ADD1/SREBP1 activates PPARγ through the production of endogenous ligand, Proc. Natl. Acad. Sci. U. S. A 95 (1998) 4333–4337. [PubMed: 9539737]

[36]. Takahashi S, Tanaka N, Fukami T, Xie C, Yagai T, Kim D, Velenosi TJ, Yan T, Krausz KW, Levi M, Gonzalez FJ, Role of farnesoid X receptor and bile acids in hepatic tumor development, Hepatol. Commun 2 (2018) 1567–1582. [PubMed: 30556042]

[37]. Takahashi S, Tanaka N, Golla S, Fukami T, Krausz KW, Polunas MA, Weig BC, Masuo Y, Xie C, Jiang C, Gonzalez FJ, Farnesoid X receptor protects against low-dose carbon tetrachloride-induced liver injury through the taurocholate-JNK pathway, Toxicol. Sci 158 (2017) 334–346. [PubMed: 28505368]

[38]. Heuman DM, Quantitative estimation of the hydrophilic-hydrophobic balance of mixed bile salt solutions, J. Lipid Res. 30 (1989) 719–730. [PubMed: 2760545]

[39]. Lee JM, Wagner M, Xiao R, Kim KH, Feng D, Lazar MA, Moore DD, Nutrient-sensing nuclear receptors coordinate autophagy, Nature 516 (2014) 112–115. [PubMed: 25383539]

[40]. Smit JJ, Schinkel AH, Oude Elferink RP, Groen AK, Wagenaar E, van Deemter L, Mol CA, Ottenhoff R, van der Lugt NM, van Roon MA, et al., Homozygous disruption of the murine mdr2 P-glycoprotein gene leads to a complete absence of phospholipid from bile and to liver disease, Cell 75 (1993) 451–462. [PubMed: 8106172]

[41]. Yu L, Gupta S, Xu F, Liverman AD, Moschetta A, Mangelsdorf DJ, Repa JJ, Hobbs HH, Cohen JC, Expression of ABCG5 and ABCG8 is required for regulation of biliary cholesterol secretion, J. Biol. Chem 280 (2005) 8742–8747. [PubMed: 15611112]

[42]. Matsubara T, Li F, Gonzalez FJ, FXR signaling in the enterohepatic system, Mol. Cell. Endocrinol 368 (2013) 17–29. [PubMed: 22609541]

[43]. Goodwin B, Jones SA, Price RR, Watson MA, McKee DD, Moore LB, Galardi C, Wilson JG, Lewis MC, Roth ME, Maloney PR, Willson TM, Kliewer SA, A regulatory cascade of the nuclear receptors FXR, SHP-1, and LRH-1 represses bile acid biosynthesis, Mol. Cell 6 (2000) 517–526. [PubMed: 11030332]

[44]. De Fabiani E, Mitro N, Anzulovich AC, Pinelli A, Galli G, Crestani M, The negative effects of bile acids and tumor necrosis factor-alpha on the transcription of cholesterol 7α-hydroxylase gene (CYP7A1) converge to hepatic nuclear factor-4: a novel mechanism of feedback regulation of bile acid synthesis mediated by nuclear receptors, J. Biol. Chem 276 (2001) 30708–30716. [PubMed: 11402042]

[45]. Li F, Patterson AD, Krausz KW, Tanaka N, Gonzalez FJ, Metabolomics reveals an essential role for peroxisome proliferator-activated receptor α in bile acid homeostasis, J. Lipid Res. 53 (2012) 1625–1635. [PubMed: 22665165]

[46]. Liu A, Krausz KW, Fang ZZ, Brocker C, Qu A, Gonzalez FJ, Gemfibrozil disrupts lysophosphatidylcholine and bile acid homeostasis via PPARα and its relevance to hepatotoxicity, Arch. Toxicol 88 (2014) 983–996. [PubMed: 24385052]

[47]. Kok T, Bloks VW, Wolters H, Havinga R, Jansen PL, Staels B, Kuipers F, Peroxisome proliferator-activated receptor alpha (PPARalpha)-mediated regulation of multidrug resistance 2 (Mdr2) expression and function in mice, Biochem. J 369 (2003) 539–547. [PubMed: 12381268]

[48]. Cheng X, Klaassen CD, Critical role of PPAR-alpha in perfluorooctanoic acid- and perfluorodecanoic acid-induced downregulation of Oatp uptake transporters in mouse livers, Toxicol. Sci 106 (2008) 37–45. [PubMed: 18703564]

[49]. Li G, Brocker CN, Xie C, Yan T, Noguchi A, Krausz KW, Xiang R, Gonzalez FJ, Hepatic peroxisome proliferator-activated receptor alpha mediates the major metabolic effects of Wy-14643, J. Gastroenterol. Hepatol 33 (2018) 1138–1145. [PubMed: 29141109]

[50]. Ghonem NS, Assis DN, Boyer JL, Fibrates and cholestasis, Hepatology 62 (2015) 635–643. [PubMed: 25678132]

[51]. Chai J, He Y, Cai SY, Jiang Z, Wang H, Li Q, Chen L, Peng Z, He X, Wu X, Xiao T, Wang R, Boyer JL, Chen W, Elevated hepatic multidrug resistance-associated protein 3/ATP-binding cassette subfamily C 3 expression in human obstructive cholestasis is mediated through tumor necrosis factor alpha and c-Jun NH2-terminal kinase/stress-activated protein kinase-signaling pathway, Hepatology 55 (2012) 1485–1494. [PubMed: 22105759]

[52]. De Fabiani E, Mitro N, Gilardi F, Caruso D, Galli G, Crestani M, Coordinated control of cholesterol catabolism to bile acids and of gluconeogenesis via a novel mechanism of transcription regulation linked to the fasted-to-fed cycle, J. Biol. Chem 278 (2003) 39124–39132. [PubMed: 12865425]

[53]. Kong B, Wang L, Chiang JY, Zhang Y, Klaassen CD, Guo GL, Mechanism of tissue-specific farnesoid X receptor in suppressing the expression of genes in bile-acid synthesis in mice, Hepatology 56 (2012) 1034–1043. [PubMed: 22467244]

[54]. Patankar JV, Wong CK, Morampudi V, Gibson WT, Vallance B, Ioannou GN, Hayden MR, Genetic ablation of Cyp8b1 preserves host metabolic function by repressing steatohepatitis and altering gut microbiota composition, Am. J. Physiol. Endocrinol. Metab 314 (2018) E418–E432. [PubMed: 29066462]

[55]. Chevre R, Trigueros-Motos L, Castano D, Chua T, Corliano M, Patankar JV, Sng L, Sim L, Juin TL, Carissimo G, Ng LFP, Yi CNJ, Eliathamby CC, Groen AK, Hayden MR, Singaraja RR, Therapeutic modulation of the bile acid pool by Cyp8b1 knockdown protects against nonalcoholic fatty liver disease in mice, FASEB J. 32 (2018) 3792–3802. [PubMed: 29481310]

[56]. Pathak P, Chiang JYL, Sterol 12α-hydroxylase aggravates dyslipidemia by activating the ceramide/mTORC1/SREBP1C pathway via FGF21 and FGF15, Gene Expr. (2019).

[57]. Preidis GA, Kim KH, Moore DD, Nutrient-sensing nuclear receptors PPARα and FXR control liver energy balance, J. Clin. Invest 127 (2017) 1193–1201. [PubMed: 28287408]

[58]. Bodewes FAJA, Wouthuyzen-Bakker M, Verkade HJ, Chapter 41 - Persistent Fat Malabsorption in Cystic Fibrosis, in: Watson RR (Ed.), Diet and Exercise in Cystic Fibrosis, Academic Press, Boston, 2015, pp. 373–381.

[59]. Day AP, Feher MD, Chopra R, Mayne PD, The effect of bezafibrate treatment on serum alkaline phosphatase isoenzyme activities, Metabolism 42 (1993) 839–842. [PubMed: 8102192]

[60]. Dai M, Yang J, Xie M, Lin J, Luo M, Hua H, Xu G, Lin H, Song D, Cheng Y, Guo B, Zhao J, Gonzalez FJ, Liu A, Inhibition of JNK signalling mediates PPARα-dependent protection against intrahepatic cholestasis by fenofibrate, Br. J. Pharmacol 174 (2017) 3000–3017. [PubMed: 28646549]

[61]. Zhao Q, Yang R, Wang J, Hu DD, Li F, PPARα activation protects against cholestatic liver injury, Sci. Rep 7 (2017) 9967. [PubMed: 28855630]

[62]. Weiskirchen R, Weiskirchen S, Tacke F, Recent advances in understanding liver fibrosis: bridging basic science and individualized treatment concepts, F1000Res 7 (2018).

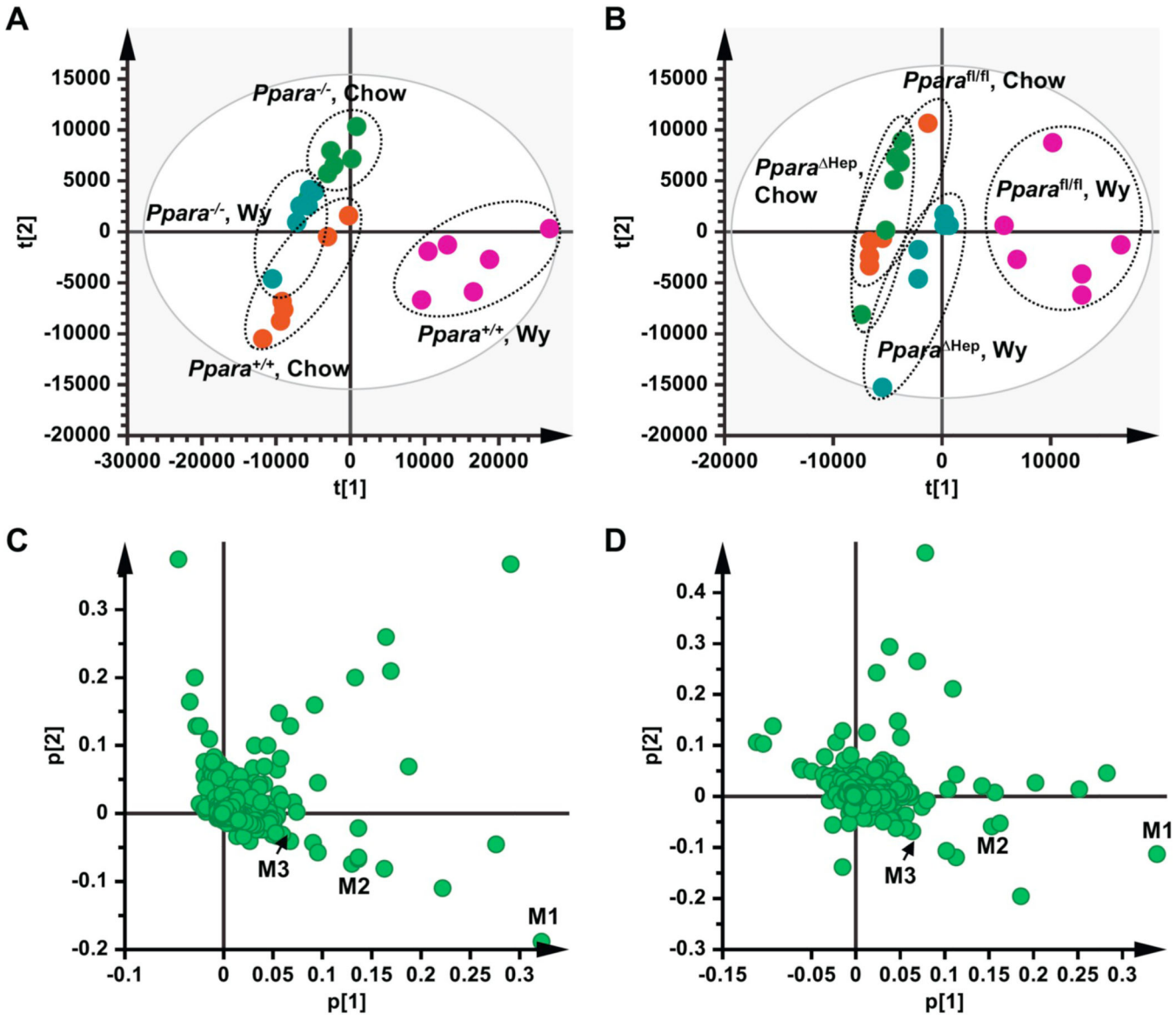

Fig. 1.

Multivariate data analysis and metabolite identification in serum of chow- and Wy-treated mice by UPLC-Q/TOFMS analysis. A. Scores plot of serum metabolome in chow- and Wy-treated *Ppara*$^{+/+}$ and *Ppara*$^{-/-}$ mice as determined by PCA. B. Scores plot of serum metabolome in chow- and Wy-treated *Ppara*$^{fl/fl}$ and *Ppara*$^{\Delta Hep}$ mice as determined by PCA. C. Loading scatter plot for PCA of serum metabolome in the chow- and Wy-treated *Ppara*$^{+/+}$ and *Ppara*$^{-/-}$ mice. D. Loading scatter plot for PCA of serum metabolome in the chow- and Wy-treated *Ppara*$^{fl/fl}$ and *Ppara*$^{\Delta Hep}$ mice. Each point represents an individual mouse serum sample (A, B) or unique ion (C, D). Ions labeled M1–M3 contribute to agonist-dependent PCA separation. The t[1] and t[2] correspond to principal components 1 and 2, respectively. The p[1] values represent the relative abundance of the ions and p[2] values represent the interclass difference. n = 6/group.

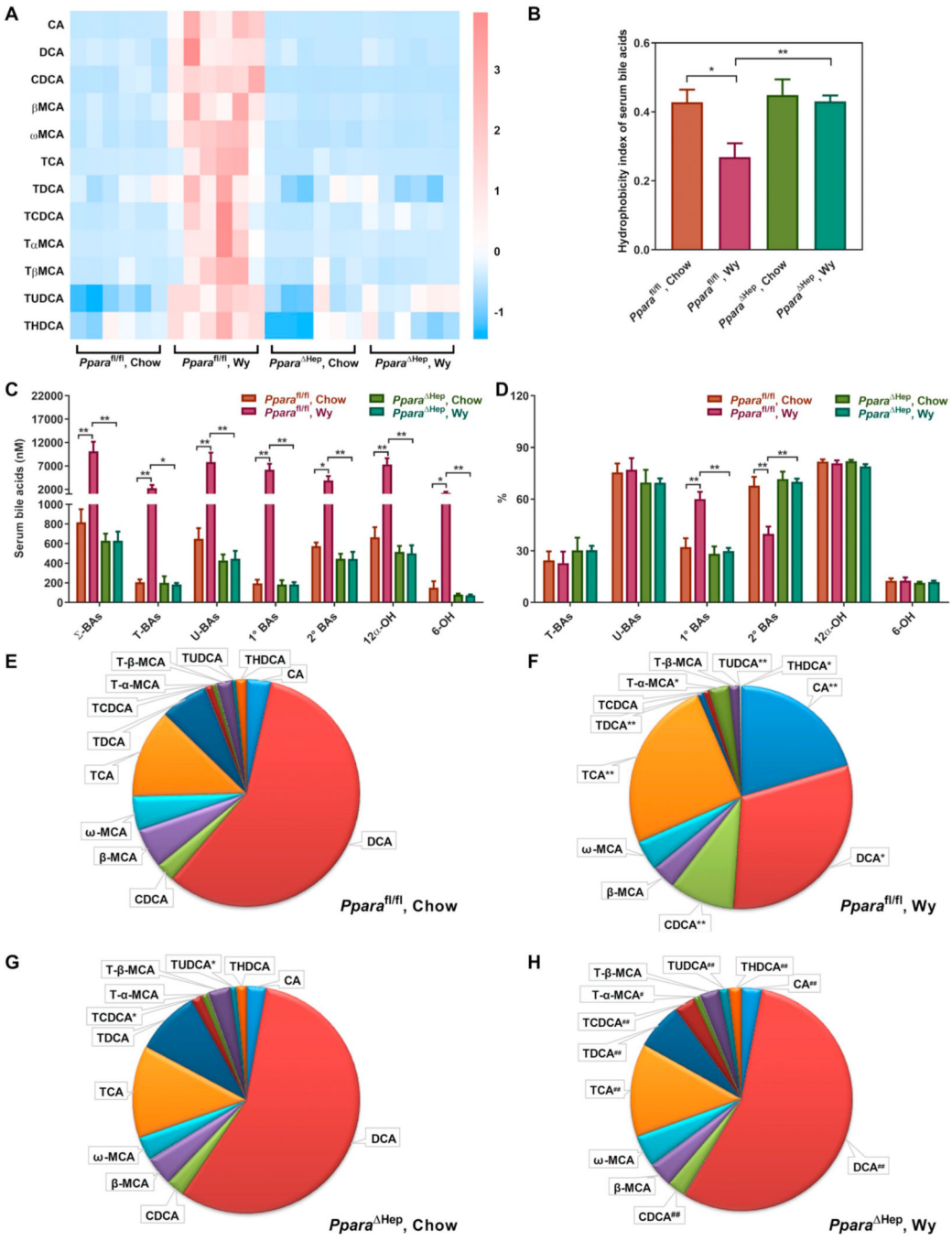

Fig. 2.

Effect of Wy on serum BA composition in *Ppara*$^{fl/fl}$ and *Ppara*$^{\Delta Hep}$ mice. A. Heat map of individual BA levels. B. Hydrophobicity index of serum bile acids. C. Total concentration of different BA classes. D. Relative percentage of different BA classes to total BAs. E. Relative fraction of individual BAs in serum of chow-treated *Ppara*$^{fl/fl}$ mice. F. Relative fraction of individual BAs in serum of Wy-treated *Ppara*$^{fl/fl}$ mice. G. Relative fraction of individual BAs in serum of Chow-treated *Ppara*$^{\Delta Hep}$ mice. H. Relative fraction of individual BAs in serum of Wy-treated *Ppara*$^{\Delta Hep}$ mice. Σ-BAs, total BAs. T-BAs, taurine-conjugated BAs. U-BAs,

unconjugated BAs. 1° BAs, primary BAs. 2° BAs, secondary BAs. 12α-OH, 12α-hydroxylated BAs. 6-OH, 6-hydroxylated BAs. Data are presented as mean ± SEM; $n = 6$/group. *$P < 0.05$ or **$P < 0.01$, by one-way ANOVA followed by Tukey's *post-hoc* correction.

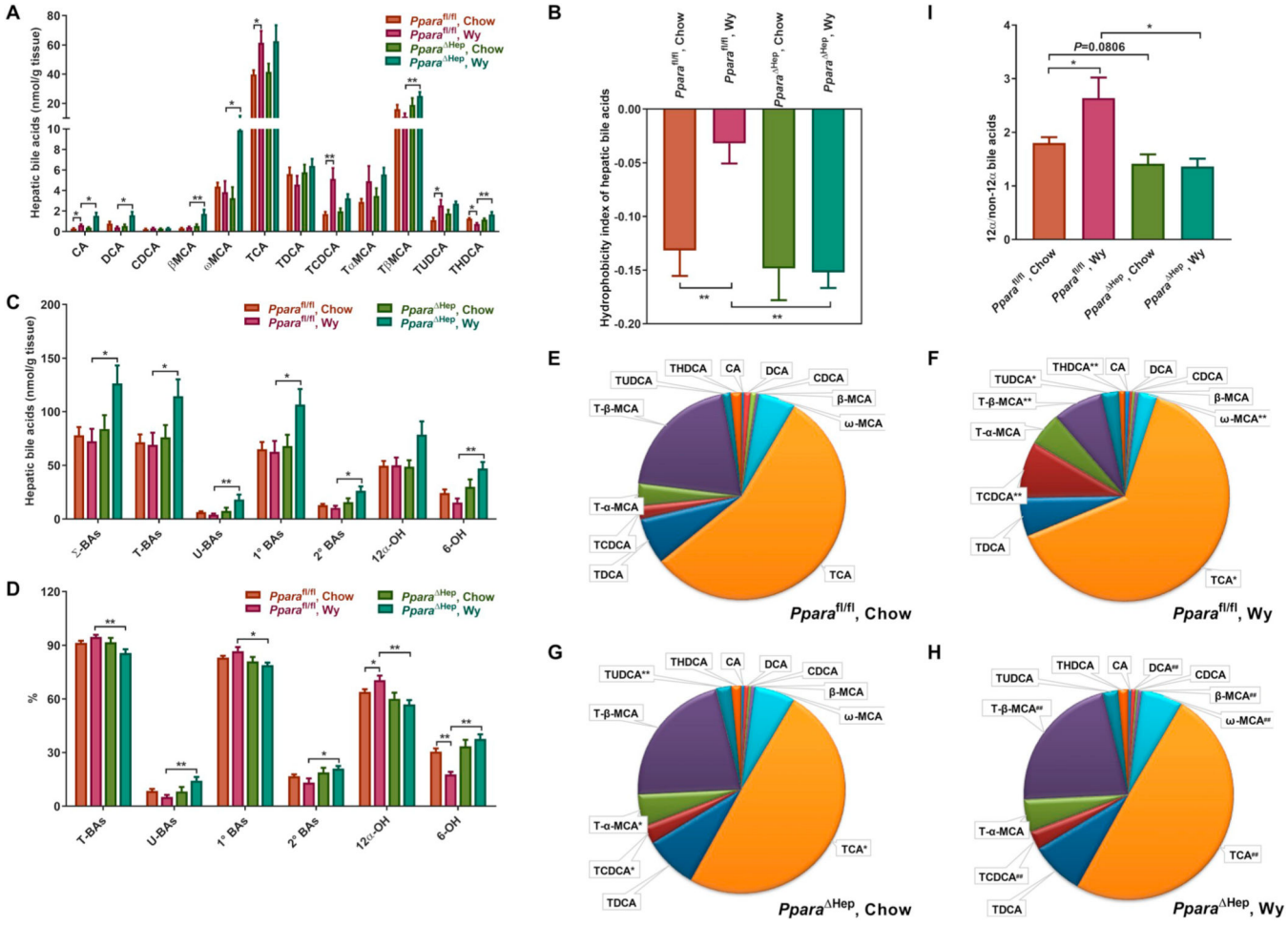

Fig. 3.

Effect of Wy on hepatic BA composition in *Ppara*$^{fl/fl}$ and *Ppara*$^{\Delta Hep}$ mice. A. Heat map of individual BA levels. B. Hydrophobicity index of hepatic bile acids. C. Total concentration of different BA classes. D. Relative percentage of different BA classes to total BAs. E. Relative fraction of individual BAs in livers of chow-fed *Ppara*$^{fl/fl}$ mice. F. Relative fraction of individual BAs in livers of Wy-treated *Ppara*$^{fl/fl}$ mice. G. Relative fraction of individual BAs in livers of chow-fed *Ppara*$^{\Delta Hep}$ mice. H. Relative fraction of individual BAs in livers of Wy-treated *Ppara*$^{\Delta Hep}$ mice. E. 12α-OH/non-12α-OH BAs ratio. Σ-BAs, total BAs. T-BAs, taurine-conjugated BAs. U-BAs, unconjugated BAs. 1° BAs, primary BAs. 2° BAs, secondary BAs. 12α-OH, 12α-hydroxylated BAs. 6-OH, 6-hydroxylated BAs. Data are presented as mean ± SEM; n = 6/group. *P < 0.05 or **P < 0.01, by one-way ANOVA followed by Tukey's *post-hoc* correction.

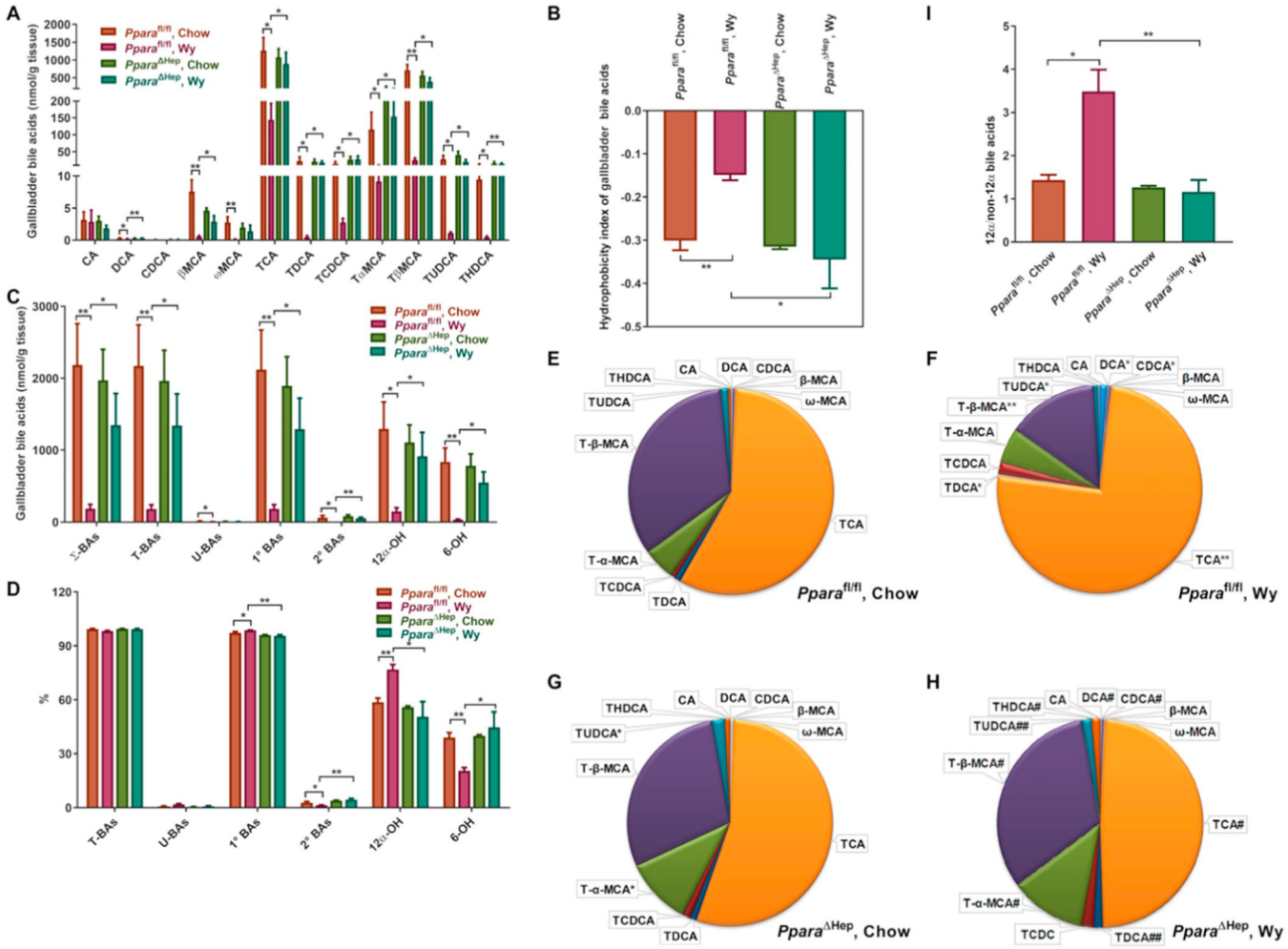

Fig. 4.

Effect of Wy on BA composition in gallbladders of *Ppara*$^{fl/fl}$ and *Ppara*$^{\Delta Hep}$ mice. A. Heat map of individual BA levels. B. Hydrophobicity index of bile acids in gallbladders. C. Total concentration of different BA classes. D. Relative percentage of different BA classes to total BAs. E. Relative fraction of individual BAs in gallbladders of chow-fed *Ppara*$^{fl/fl}$ mice. F. Relative fraction of individual BAs in gallbladders of Wy-treated *Ppara*$^{fl/fl}$ mice. G. Relative fraction of individual BAs in gallbladders of chow-fed *Ppara*$^{\Delta Hep}$ mice. H. Relative fraction of individual BAs in gallbladders of Wy-treated *Ppara*$^{\Delta Hep}$ mice. I. 12α-OH/non-12α-OH BAs ratio. Σ-BAs, total BAs. T-BAs, taurine-conjugated BAs. U-BAs, unconjugated BAs. 1° BAs, primary BAs. 2° BAs, secondary BAs. 12α-OH, 12α-hydroxylated BAs. 6-OH, 6-hydroxylated BAs. Data are presented as mean ± SEM; n = 3–4/group. *P < 0.05 or **P < 0.01, by one-way ANOVA followed by Tukey's *post-hoc* correction.

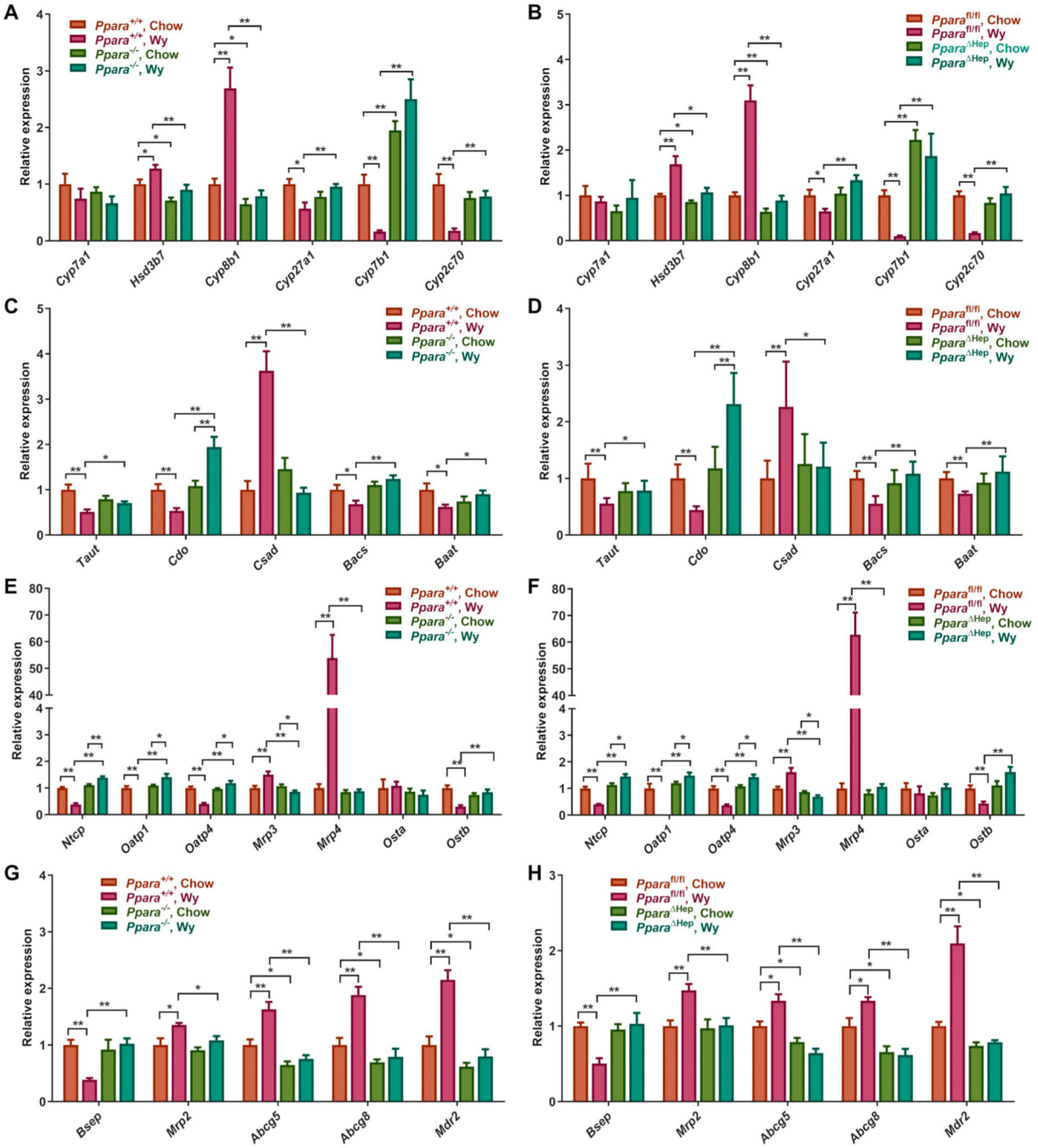

Fig. 5.

Wy treatment alters hepatic expression of genes involved in BA synthesis, conjugation, and transport. A. mRNA levels of genes involved in BA synthesis in chow- and Wy-treated *Ppara* $^{+/+}$ and *Ppara*$^{-/-}$ mice. B. mRNA levels of genes involved in BA synthesis in chow- and Wy-treated *Ppara*$^{fl/fl}$ and *Ppara*$^{\Delta Hep}$ mice. C. mRNA levels of genes involved in taurine conjugation in chow- and Wy-treated *Ppara*$^{+/+}$ and *Ppara*$^{-/-}$ mice. D. mRNA levels of genes involved in taurine conjugation in chow- and Wy-treated *Ppara*$^{fl/fl}$ and *Ppara*$^{\Delta Hep}$ mice. E. mRNA levels of genes related to the BA sinusoidal transporters in chow- and Wy-treated

Ppara$^{+/+}$ and *Ppara*$^{-/-}$ mice. F. mRNA levels of genes related to the BA sinusoidal transporters in chow- and Wy-treated *Ppara*$^{fl/fl}$ and *Ppara*$^{\Delta Hep}$ mice. G. mRNA levels of genes related to the BA canalicular transporters in chow- and Wy-treated *Ppara*$^{+/+}$ and *Ppara*$^{-/-}$ mice. H. mRNA levels of genes related to the BA canalicular transporters in chow- and Wy-treated *Ppara*$^{fl/fl}$ and *Ppara*$^{\Delta Hep}$ mice. Data are presented as mean ± SEM; $n = 6$/group. *$P < 0.05$ or **$P < 0.01$, by one-way ANOVA followed by Tukey's *post-hoc* correction.

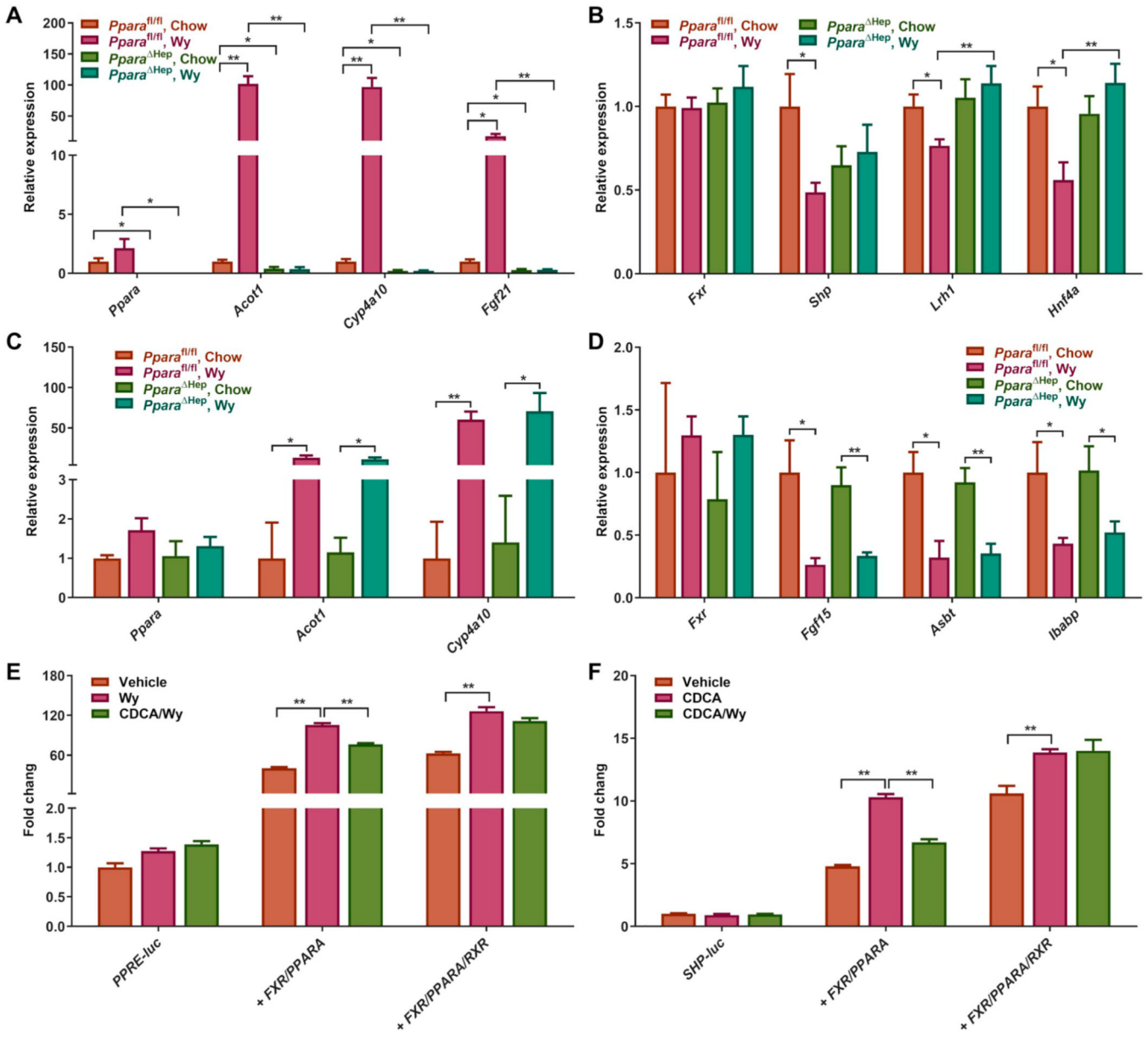

Fig. 6.

PPARα activation by Wy treatment suppresses FXR signaling through RXRα competition. A. Hepatic mRNA expression of PPARα and its target genes. B. Hepatic mRNA expression of genes involved in regulating BA homeostasis. C. Intestinal *Ppara* mRNA expression and its target genes. D. Intestinal mRNA expression of genes involved in regulating BA homeostasis. E. Luciferase activity of vehicle-, Wy-, and CDCA-treated AML12 cells co-transfected with PPRE-luc reporter and empty vector, FXR, PPARα, and/or RXRα expression vectors. F. Luciferase activity of vehicle-, CDCA-, and Wy-14,643-treated AML12 cells co-transfected with SHP-luc reporter and empty vector, FXR, PPARα and/or RXRα expression vectors. Data are presented as mean ± SEM; $n = 6$/group. *$P < 0.05$ or **$P < 0.01$, by one-way ANOVA followed by Tukey's *post-hoc* correction.

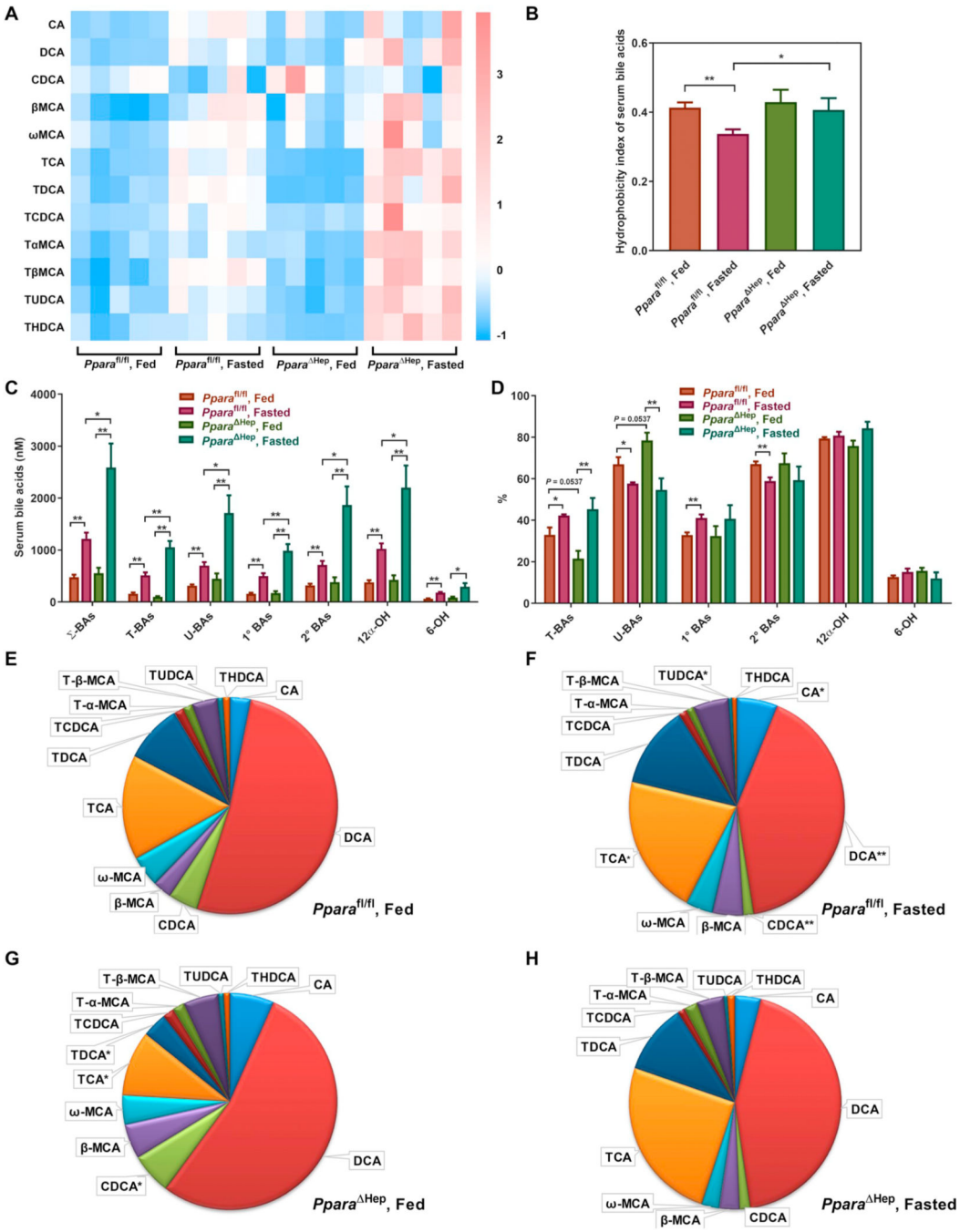

Fig. 7.

Effect of fasting on serum BA composition in *Ppara*$^{fl/fl}$ and *Ppara*$^{\Delta Hep}$ mice. A. Heat map of individual BA levels. B. Hydrophobicity index of serum bile acids. C. Total concentration of different BA classes. D. Relative percentage of different BA classes to total BAs. E. Relative fraction of individual BAs in serum of fed *Ppara*$^{fl/fl}$ mice. F. Relative fraction of individual BAs in serum of fasted *Ppara*$^{fl/fl}$ mice. G. Relative fraction of individual BAs in serum of fed *Ppara*$^{\Delta Hep}$ mice. H. Relative fraction of individual BAs in serum of fasted *Ppara*$^{\Delta Hep}$ mice. Σ-BAs, total BAs. T-BAs, taurine-conjugated BAs. U-BAs, unconjugated BAs. 1° BAs,

primary BAs. 2° BAs, secondary BAs. 12α-OH, 12α-hydroxylated BAs. 6-OH, 6-hydroxylated BAs. Data are presented as mean ± SEM; $n = 6$/group. *$P < 0.05$ or **$P < 0.01$, by one-way ANOVA followed by Tukey's *post-hoc* correction.

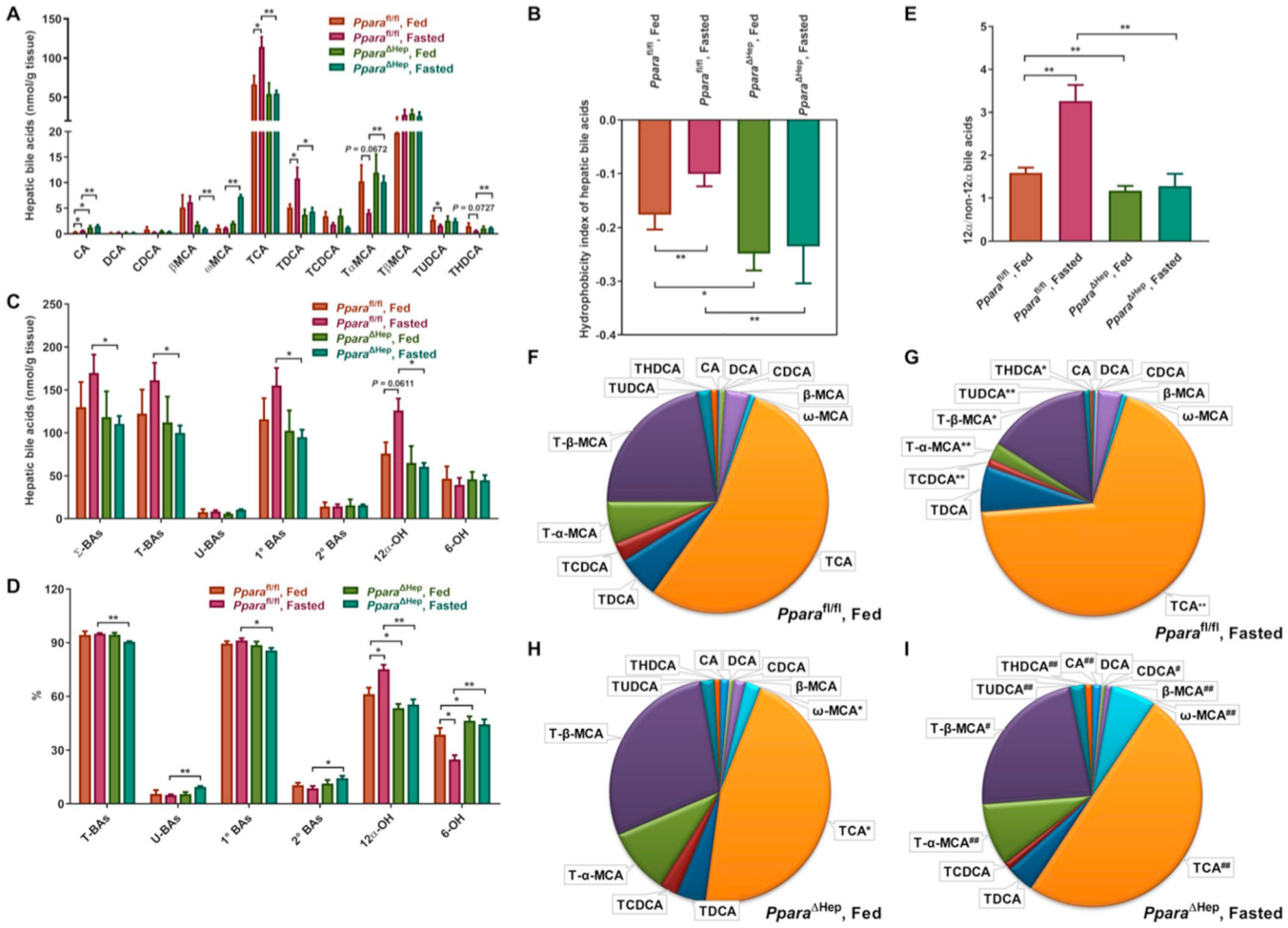

Fig. 8.

Effect of fasting on hepatic BA composition in *Ppara*$^{fl/fl}$ and *Ppara*$^{\Delta Hep}$ mice. A. Heat map of individual BA levels. B. Hydrophobicity index of hepatic bile acids. C. Total concentration of different BA classes. D. Relative percentage of different BA classes to total BAs. E. Relative fraction of individual BAs in livers of fed *Ppara*$^{fl/fl}$ mice. F. Relative fraction of individual BAs in livers of fasted *Ppara*$^{fl/fl}$ mice. G. Relative fraction of individual BAs in livers of fed *Ppara*$^{\Delta Hep}$ mice. H. Relative fraction of individual BAs in livers of fasted *Ppara*$^{\Delta Hep}$ mice. I. 12α-OH/non-12α-OH BAs ratio. Σ-BAs, total BAs. T-BAs, taurine-conjugated BAs. U-BAs, unconjugated BAs. 1° BAs, primary BAs. 2° BAs, secondary BAs. 12α-OH, 12α-hydroxylated BAs. 6-OH, 6-hydroxylated BAs. Data are presented as mean ± SEM; $n = 6$/group. *$P < 0.05$ or **$P < 0.01$, by one-way ANOVA followed by Tukey's *post-hoc* correction.

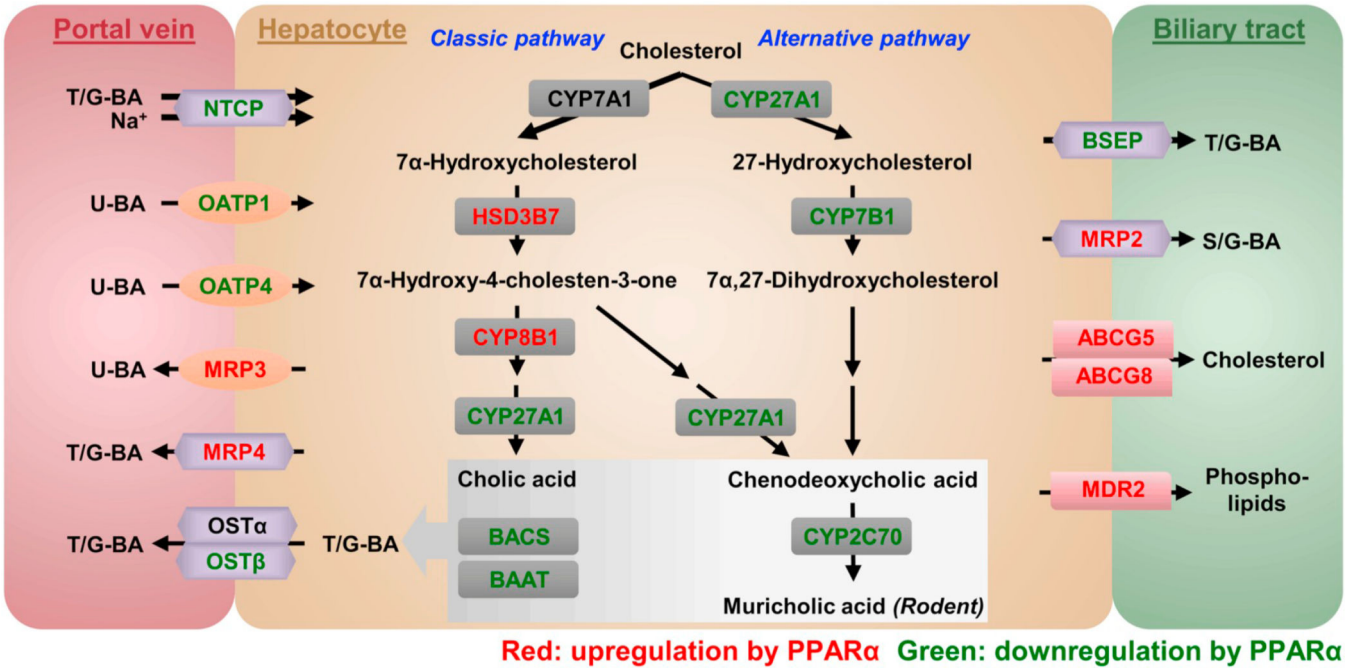

Fig. 9.

Mechanism for hepatocyte PPARα activation on BA synthesis and transport regulation. PPARα activation within hepatocytes by Wy represses both hepatic BA uptake mediated by NTCP and OATPs and canalicular BA efflux mediated by BSEP, while increases sinusoidal BA efflux by induction of MRP3 and MRP4. The overall effect is elevated circulating BAs. PPARα activation also induces the expression of CYP8B1 which leads to the increased levels of CA and TCA in classic pathway as well as downregulates the expression of CYP27A1 and CYP7B1 in alternative BA synthesis. These changes result in an increased 12α-OH/non-12α-OH BAs ratio. The reduced expression of CYP2C70 decreases the synthesis of FXR antagonist pool consisting of TαMCA and TβMCA. T/G-BA, taurine/glycine-conjugated BA. U-BA, unconjugated BA. S/G-BA, sulfate or glucuronide-conjugated BA. The proteins in red are induced by PPARα activation and the proteins in green are suppressed by PPARα activation. (For interpretation of the references to colour in this figure legend, the reader is referred to the web version of this article.)

Table 1

Serum metabolite ions identified in the negative mode that were significantly increased in Wy-treated *Ppara*$^{+/+}$ and *Ppara*$^{fl/fl}$ mice.

	m/z	Rt	*Ppara*$^{+/+}$, Wy			Ppara$^{fl/fl}$, Wy			Metabolite
			P[1]	P[2]	VIP	P[1]	P[2]	VIP	
M1	514.284	10.3	0.3218	−0.1882	11.1	0.3397	−0.1139	11.4	TCA
M2	514.284	7.2	0.1306	−0.0751	4.6	0.1527	−0.0587	5.4	TβMCA
M3	391.285	18.8	0.0677	−0.0398	2.8	0.0801	−0.0095	3.4	DCA
M4	514.284	6.7	0.0551	−0.0338	2.0	0.0565	−0.0355	2.5	TαMCA
M5	498.289	13.6	0.0522	−0.0295	1.8	0.0362	−0.0170	2.4	TDCA
M6	407.280	12.2	0.0499	−0.0309	1.7	0.0754	−0.0206	1.7	CA
M7	498.288	13.0	0.0389	−0.0227	1.5	0.0415	−0.0170	1.6	TCDCA
M8	498.288	9.8	0.0244	−0.0150	1.1	0.0294	−0.0179	1.1	TUDCA
M9	498.288	10.0	0.0213	−0.0049	1.0	0.0215	−0.0208	1.0	THDCA